



JGR Atmospheres

RESEARCH ARTICLE

10.1029/2018JD028321

Key Points:

- Large differences in ice cloud optical depths are found between CALIPSO and ground-based Raman lidars (RLs)
- The relationship between lidar ratio and temperature used in the CALIPSO Version 4 is different from that based on the RLs
- The optical depths can be reconciled with consistent resolution, lidar ratio, transparent definition, and considering lidar sensitivity

Correspondence to:

K. A. Balmes,
kbalmes@uw.edu

Citation:

Balmes, K. A., Fu, Q., & Thorsen, T. J. (2019). Differences in ice cloud optical depth from CALIPSO and ground-based Raman lidar at the ARM SGP and TWP sites. *Journal of Geophysical Research: Atmospheres*, 124, 1755–1778. <https://doi.org/10.1029/2018JD028321>

Received 12 JAN 2018

Accepted 13 JAN 2019

Accepted article online 16 JAN 2019

Published online 12 FEB 2019

Differences in Ice Cloud Optical Depth From CALIPSO and Ground-Based Raman Lidar at the ARM SGP and TWP Sites

K. A. Balmes¹ , Q. Fu¹ , and T. J. Thorsen²

¹Department of Atmospheric Sciences, University of Washington, Seattle, WA, USA, ²NASA Langley Research Center, Hampton, VA, USA

Abstract Ice cloud column optical depths from the Cloud-Aerosol Lidar and Infrared Pathfinder Satellite Observations (CALIPSO) satellite and ground-based Raman lidars (RLs) at the Atmospheric Radiation Measurement (ARM) Southern Great Plains (SGP) and Tropical Western Pacific (TWP) sites are compared for 8 and 4 years, respectively. The cloudy mean ice cloud column optical depths from CALIPSO Version 4 data product with a horizontal resolution of 5 km are 78% (63%) larger than those from the RLs with a resolution of 10 min/30 m at SGP (TWP) for collocated transparent profiles. The main difference at SGP is caused by the lidar ratio that for CALIPSO is related to its treatment of the multiple scattering factor. The main difference at TWP is caused by the averaging resolution. Large differences in the optical depth distribution between the CALIPSO and RL are found for small optical depths at both sites, which are due to optically very thin clouds only detectable by the RLs. The differences in ice cloud column optical depth distributions and their mean values between the CALIPSO and RL can largely be reconciled over both sites after accounting for the averaging resolutions, lidar ratios along with the CALIPSO multiple scattering factor treatment, sensitivity to optically very thin ice clouds, and definition of transparent profiles. This work also examines in detail the lidar ratios that are directly observed by the RLs, which does not support the temperature-dependent parameterizations of ice cloud lidar ratio and multiple scattering factor used in CALIPSO's Version 4 data product.

1. Introduction

Ice clouds are ubiquitous and strongly influence the global radiative energy budget (e.g., Liou, 1986). Ice cloud radiative effects strongly depend on ice cloud optical properties (e.g., Fu & Liou, 1993; Platt & Harshvardhan, 1988) making observations of these properties critical for understanding the impacts of ice clouds on the climate (e.g., Fu et al., 2002; Stephens et al., 1990). The launch of the Cloud-Aerosol Lidar with Orthogonal Polarization (CALIOP) on board the Cloud-Aerosol Lidar and Infrared Pathfinder Satellite Observations (CALIPSO) has provided new insights into the global properties of ice clouds with information on their vertical structures (Winker et al., 2010). Near-global climatology for ice cloud occurrence from CALIPSO has characterized ice clouds worldwide without the limitations of passive instruments and sparse field observations (Fu et al., 2007; Sassen et al., 2008).

Ground-based remote sensing provides continuous measurements with large sample sizes to evaluate satellite remote sensing cloud properties (e.g., Campbell et al., 2002; Hollars et al., 2004; Sassen & Campbell, 2001; Thorsen et al., 2011, 2013). The ground-based Raman lidars (RLs; Ferrare et al., 2006; Goldsmith et al., 1998; Newsom, 2009) at the Atmospheric Radiation Measurement Program (ARM; Ackerman & Stokes, 2003) sites have recently been shown to perform well for cloud detection, particularly for high clouds (Thorsen et al., 2013, 2015; Thorsen & Fu, 2015). More importantly, the RL is capable of directly measuring the lidar ratio, the ratio of particulate extinction to backscatter, by independently measuring both particulate extinction and particulate backscatter (Ansmann et al., 1990), which we refer to as the Raman method. The lidar ratio often must be assumed for backscatter lidar systems (e.g., CALIPSO) in order to obtain the extinction coefficient and hence the optical depth. In the CALIPSO Version 3 data product, an ice cloud lidar ratio of 25 sr was used for nearly all ice cloud retrievals (Winker et al., 2009). One option for CALIPSO to improve beyond an assumed lidar ratio is to use the transmission method when clear sky bounds a feature layer to constrain the retrieval (Yang et al., 2010). However, it is the effective lidar ratio (i.e., the product of the lidar ratio and multiple scattering factor) that is derived

from the transmission method, requiring a multiple scattering factor in order to obtain the lidar ratio. The multiple scattering factor accounts for contributions from multiple scattering to the apparent two-way transmittance (Garnier et al., 2015; Platt, 1973) and was a constant of 0.6 for all ice cloud retrievals in the CALIPSO Version 3. Recently, CALIPSO's version 4.10 data product features the parameterizations of ice cloud multiple scattering factor and then lidar ratio in terms of cloud centroid temperature. The parameterization is based on the transmission method using 3 years (2008, 2010, and 2013) of nighttime only randomly oriented ice particle data acquired over the ocean between 82°S and 82°N (Garnier et al., 2015; Young et al., 2018) although the parameterization is extended for both daytime and nighttime over both the ocean and land. The development of a new treatment of ice cloud lidar ratios was in part motivated by comparisons of CALIPSO and Moderate Resolution Imaging Spectroradiometer (MODIS) ice cloud optical depth, which showed that MODIS optical depths are larger than CALIPSO Version 3 optical depths by a factor of 2 (Holz et al., 2016). The observations of high clouds from RL with directly measured lidar ratios provide a useful data set for examining CALIPSO retrievals, and they also provide an opportunity to investigate differences between lidar ratios derived from the Raman and transmission methods.

In this study, the ground-based ARM RLs are utilized to investigate ice cloud lidar ratios and optical depths at the ARM Southern Great Plains (SGP) and Tropical Western Pacific (TWP) sites. The temperature-dependent parameterizations of ice cloud lidar ratio and multiple scattering factor that are used in the CALIPSO Version 4 data product are evaluated. Ice cloud detection and optical depths from the CALIPSO Version 4 data product are compared with those from the RLs. We examine the role of lidar ratio and multiple scattering factor used in CALIPSO in interpreting the difference in the retrieved ice cloud optical depth between the CALIPSO and the RL. We also examine the impact of spatial and temporal averaging, lidar detection sensitivity and the transparent profile definition on the retrieved ice cloud optical depth.

Section 2 outlines the ground-based RL and CALIPSO data sets, defines the transparent profiles for the comparison, and describes the Raman and transmission methods for the lidar ratio. Section 3 examines the relationship of the lidar ratio with temperature for ice clouds from the RL and compares it with that from CALIPSO. The dependence of the CALIPSO multiple scattering factor on temperature is also examined. Section 4 explores the impact of the lidar ratio and the temporal and vertical averages on the RL retrieved ice cloud optical depth. Section 5 compares the CALIPSO and RL ice cloud detection and retrieved optical depths. Section 6 summarizes and concludes all findings presented.

2. Data Sets and Methods

2.1. ARM RL

The Department of Energy (DOE) ARM operates ground-based RLs as part of its permanent and mobile deployment missions (Ferrare et al., 2006; Goldsmith et al., 1998; Newsom, 2009). Originally deployed in 1998 at the SGP site, the RL operates at 355 nm during nighttime and daytime. The RL contains detection channels for elastic-scattered light and Raman-scattered light from nitrogen, water vapor, and two temperature channels (Goldsmith et al., 1998). The RLs intrinsically separate particulate and molecular signals allowing for direct retrievals of extinction and lidar ratios. A recently developed feature detection and extinction (FEX) retrieval algorithm (Thorsen et al., 2015; Thorsen & Fu, 2015) provides cloud and aerosol detection and extinction profiles from the RL observations. The studies by Thorsen et al. (2015) and Thorsen and Fu (2015) provide a large database of directly retrieved lidar ratios, giving the unique opportunity to explore the relationship of the lidar ratio with temperature and the effects on optical depth retrieval.

Two locations used in this study are the SGP site located in Lamont, Oklahoma (36.61°N, 97.49°W) and the TWP site located in Darwin, Australia (12.43°S, 130.89°E). The time period studied extends from 1 August 2008 to 31 August 2016 at SGP and for the full lifetime of operation at TWP from 15 December 2010 to 1 January 2015 before it was moved to the ARM Eastern North Atlantic site located on Graciosa Island, Azores. The nominal temporal and vertical resolutions (averaging) used are 10 min and 30 m and the effect of modifying these resolutions is explored in sections 4 and 5.

FEX requires feature particle size for calculating the multiple scattering functions. In Thorsen et al. (2015) and Thorsen and Fu (2015), the ice particle size was determined by a power law fit between effective radius and particulate extinction from in situ data in Fu (1996). More recent parameterizations of ice particle sizes

have been developed based on observations (e.g., Boudala et al., 2002; Heymsfield et al., 2014). In this study, we instead incorporate an ice particle size based on temperature from Heymsfield et al. (2014). Overall, the ice cloud effective radii are larger compared to Fu (1996), which led to larger lidar ratios and particulate extinction. However, the median percentage difference is relatively small (3–9%). More details on the differences between using the ice cloud effective radius parameterization from Fu (1996) and Heymsfield et al. (2014) are provided in Appendix A.

2.2. CALIPSO

Launched in April 2006 into a Sun-synchronous orbit, the CALIPSO provides vertical cloud and aerosol profiles as part of the A-train satellite constellation (Winker et al., 2010). The instrument relevant to this study is the near-nadir-viewing polarization sensitive lidar onboard CALIOP operating at 532 and 1,064 nm. The three data sets used in this study are the CALIPSO L2 v4.10, 5-km cloud profile product for optical depth information, CALIPSO L2 v4.10, 5-km cloud layer product for lidar ratio and multiple scattering factor information, and the CALIPSO L2 v4.10 vertical feature mask for feature detection information. Cloud layer detection is performed using a threshold algorithm described in Vaughan et al. (2009), and the extinction retrieval is outlined in Young and Vaughan (2009) with Version 4 updates highlighted in Young et al. (2018) including the new treatments of ice cloud lidar ratio and multiple scattering factor. In this analysis, cloud layer and vertical feature mask data are filtered for ice clouds with randomly-oriented ice particles using the Feature Classification Flag to avoid including ice clouds containing horizontally oriented ice particles. CALIPSO extinction retrievals are limited to those that correspond to a QC flag value of 0, 1, or 2. CALIPSO data are limited to 5° latitude by 5° longitude boxes centered over the SGP and TWP sites from 13 June 2006 to 31 August 2016, which represents the beginning of CALIPSO's data set through the end of the RL's data set.

2.3. Collocated and Transparent Profiles

In this study, RL collocated profiles are defined as those within ± 4 hr centered over a CALIPSO flyover time, while CALIPSO collocated profiles are defined as those within 5° latitude by 5° longitude box centered over the SGP and TWP sites when the RL was operational (including both nighttime and daytime). Other more restrictive collocated definitions (e.g., RL ± 2 hr and CALIPSO profiles within a 200-km radius of the SGP and TWP sites) were tested, but similar results were obtained (not shown).

Transparent profiles are defined as when the signals from both platforms pass completely through the atmosphere without becoming fully attenuated before reaching an altitude beyond clouds from the ground-based perspective and before reaching the ground from the space-borne perspective. Only including transparent profiles means that the advantages related to a given platform are leveled for a fairer comparison. For satellite-based (ground-based) lidar measurements, the advantage of sampling high (low) clouds is leveled by requiring passing through the whole atmosphere to be classified as transparent.

RL transparent profiles are defined as a signal-to-noise ratio (SNR) greater than 1 at 16 and 18 km for SGP and TWP, respectively. For all available profiles, 69% and 62% of them were transparent for resolutions of 10 m and 30 m at SGP and TWP, respectively, while for collocated profiles, 68% and 60% were transparent.

CALIPSO transparent profiles are defined as when the surface is detected at all 1/3-km pixels (single-shot resolution) within the 5-km profile (final data product resolution). The definition is to ensure that opaque cases are not mischaracterized as transparent cases by excluding profiles that are only partially transparent. Of the CALIPSO collocated profiles, 60% and 55% were transparent over SGP and TWP, respectively.

2.4. Transparent Collocated Ice Cloud Column Optical Depths

We construct ice cloud column optical depth with RL's and CALIPSO's extinction profiles. Ice cloud column optical depths here refer to integrating all ice cloud particulate extinction present within a given profile, expressed as

$$\tau_{i,c} = \int_{z_{\text{base}}}^{z_{\text{top}}} \alpha_i(z) dz, \quad (1)$$

where $\tau_{i,c}$ is the ice cloud column optical depth, α_i is ice cloud particulate extinction (km^{-1}), z_{top} (z_{base}) is the highest (lowest) ice cloud top (base) height of the atmospheric profile. We compare the ice cloud column optical depths from RL observations with CALIPSO. Column optical depths are chosen over individual

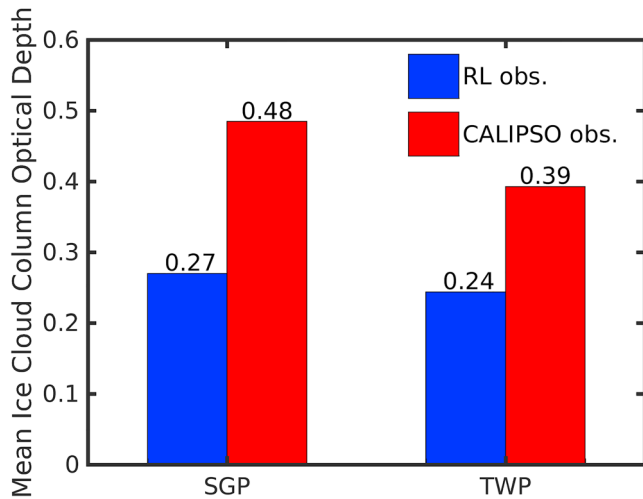


Figure 1. Mean ice cloud column optical depth of transparent collocated ice cloudy profiles for the Raman lidar (blue) and CALIPSO (red) at the SGP (left) site from August 2008 to August 2016 and at the TWP (right) site from December 2010 to January 2015. Mean values are labeled above each bar. RL = Raman lidar; CALIPSO = Cloud-Aerosol Lidar and Infrared Pathfinder Satellite Observations; SGP = Southern Great Plains; TWP = Tropical Western Pacific.

cloud layer optical depths because CALIPSO’s cloud layer data product contains scenarios when multiple cloud layers overlap vertically (Thorsen et al., 2011; Vaughan et al., 2009). Comparing cloud column optical depths also avoids the potential complications associated with different approaches for defining cloud layers.

Figure 1 shows the comparison of mean ice cloud column optical depth from the RL and CALIPSO for collocated transparent ice cloudy profiles considering both nighttime and daytime. The RL resolution is for a temporal and vertical resolution of 10 min/30 m and the CALIPSO resolution is for a horizontal resolution of 5 km and vertical resolution of 60 m. The CALIPSO horizontal resolution of 5 km is averaged from 15 CALIPSO lidar pulses, where each lidar pulse corresponds to ~0.75 s that CALIPSO traveled. Large differences exist between the two observations at both locations. The mean ice cloud column optical depths from CALIPSO are 78% and 63% larger than those from the RLs at the SGP and TWP sites, respectively. Subsequent sections will explore, in detail, the underlying causes of the large discrepancy in the ice cloud column optical depths.

2.5. Lidar Ratio From the Raman and Transmission Method

The CALIPSO cloud product estimates the lidar ratio for either constrained or unconstrained retrievals. Constrained retrievals (i.e., extinction QC flag = 1) utilize the transmission method when features are bounded by clear air (Yang et al., 2010). The constrained retrievals constrain the feature’s two-way transmittance, which results in a measure of the effective lidar ratio (i.e., the product of the lidar ratio and multiple scattering factor). Therefore, the multiple scattering factor is required to obtain the lidar ratio. Unconstrained retrievals (i.e., extinction QC flag = 0) are utilized when a constrained retrieval is not possible. Unconstrained retrievals estimate the lidar ratio based on the temperature following the V4 temperature-dependent parameterizations of lidar ratio (Young et al., 2018). For transparent collocated CALIPSO ice clouds, 50% (61%) are constrained retrievals and 50% (39%) are unconstrained retrievals for SGP (TWP). The remaining 0.3% (0.2%) for SGP (TWP) correspond to the third CALIPSO lidar ratio method, which is when the lidar ratio is reduced to successfully retrieve backscatter (i.e., extinction QC flag = 2) (Young et al., 2018).

RL FEX uses several methods for deriving lidar ratios and a “best estimate” is selected to minimize the uncertainty in the final values. Table 1 lists occurrence percentage, mean, median, standard deviation, and backscatter-weighted lidar ratio of the different methods employed for the best estimate of ice cloud lidar ratios for all profiles. The backscatter-weighted lidar ratio is defined as

$$\overline{S}_\beta = \frac{\sum_{j=1}^N S_j \beta_j}{\sum_{j=1}^N \beta_j}, \quad (2)$$

where \overline{S}_β is the backscatter-weighted lidar ratio (sr), β is the particulate backscatter (km sr^{-1}), S is the lidar ratio (sr), and N is the total number of ice cloud bins observed (i.e., N in Tables 1 and 2). Note that CALIPSO-constrained observations retrieve backscatter-weighted lidar ratios for the cloud layer. Table 2 includes the same information as Table 1 but only for transparent profiles, that is, the subset relevant to the comparison with CALIPSO. Two methods of interest to this study are the Raman method and the transmission method. The Raman

Table 1
Statistics of Lidar Ratios (Mean, Median, Standard Deviation, and Backscatter-Weighted Mean) in Units of sr From the Raman Method, Transmission Method, Interpolation, Inferred and Assumed Values Used for the Best Estimate, and Those From the Best Estimate for All Observed Profiles

Method	Percentage of total	Mean	Median	Standard deviation	Backscatter-weighted
SGP (N = 8,946,260)					
Raman	70.8%	22.1	21.6	7.4	18.0
Transmission	9.7%	23.8	22.8	9.4	21.2
Interpolation	1.0%	20.6	20.3	6.6	17.8
Inferred	16.3%	21.1	21.1	6.1	18.7
Assumed	2.2%	21.7	21.7	0.2	21.7
Best estimate	100%	22.1	21.7	7.4	18.4
TWP (N = 5,613,516)					
Raman	39.2%	27.2	27.1	5.5	24.0
Transmission	14.3%	29.9	28.1	10.4	28.2
Interpolation	1.5%	25.4	25.5	4.8	23.0
Inferred	33.6%	27.6	27.8	4.1	25.3
Assumed	11.4%	27.3	27.3	0.02	27.2
Best estimate	100%	27.8	27.3	5.9	24.6

Note. N is the total number of ice cloud bins observed by the RL (i.e., the summation of the vertical ice cloud bin numbers for all observed profiles) for which the lidar ratio statistics are calculated. The percentage of ice cloud bin retrievals corresponding to these methods for the best estimate are also given. The RL observations are from August 2008 to August 2016 for the SGP site and from December 2010 to January 2015 for the TWP site. RL = Raman lidar; SGP = Southern Great Plains; TWP = Tropical Western Pacific.

Table 2
The Same as Table 1 but for Transparent Profiles Observed by RLs

Method	Percentage of total	Mean	Median	Standard deviation	Backscatter-weighted
SGP (N = 5,346,920)					
Raman	75.1%	23.1	22.8	6.9	21.5
Transmission	12.1%	23.9	22.8	9.3	21.5
Interpolation	0.5%	22.5	22.7	6.0	21.0
Inferred	11.1%	21.7	21.6	5.6	19.9
Assumed	1.2%	21.7	21.7	0.1	21.7
Best estimate	100%	23.1	22.6	7.1	21.4
TWP (N = 3,012,843)					
Raman	30.8%	29.0	28.7	5.0	28.4
Transmission	20.9%	29.4	27.7	10.2	28.1
Interpolation	0.3%	28.9	28.8	4.5	28.8
Inferred	28.0%	28.6	28.6	3.8	28.2
Assumed	20.0%	27.3	27.3	0.02	27.3
Best estimate	100%	28.6	27.3	5.8	28.2

method uses profiles of particulate extinction and backscatter directly retrieved from the RL. The Raman method represents 71% and 39% of ice cloud bins with 10 min/30 m resolution at SGP and TWP, respectively. The Raman method is not used for all ice cloud retrievals since the weak Raman scattering process can result in unreliable noisy retrievals. The transmission method constructs a layer-averaged lidar ratio when attenuation is weaker, and clear sky bounds the feature layer, which accounts for 10% and 14% of ice cloud bins with 10-min/30-m resolution at SGP and TWP, respectively. Similar percentages are observed for transparent profiles (Table 2), with 75% and 31% for the Raman method and 12% and 21% for the transmission method at SGP and TWP, respectively. Since the transmission method is utilized in the CALIPSO retrievals, comparing the lidar ratios produced by the two methods from the RL observations becomes important for understanding the differences in retrieved ice cloud optical depth.

Additional methods used by the RLs include interpolation, inferred and assumed, which in total represent the remaining 19% and 47% of ice cloud bins at SGP and TWP, respectively. The interpolation method interpolates lidar ratios retrieved by the Raman or transmission method to nearby bins. The inferred method infers the lidar ratio derived from layer-, profile-, or daily- averaged values of all directly retrieved lidar ratios for a given feature, where directly retrieved refers to those from the Raman, transmission or interpolation methods. The assumed method uses a single climatological lidar ratio value when no other method can reliably be used. These methods are presented in detail in Thorsen and Fu (2015). Here we focus on the Raman and transmission methods because these methods are the primary methods of the RL and CALIPSO, respectively.

Figure 2 shows the probability distribution functions (PDFs) of ice cloud lidar ratios retrieved from the Raman and transmission methods based on the RL observations when used in the best estimate. Larger lidar ratios are observed over the TWP site than the SGP site from both methods. At both sites, the transmission method gives larger lidar ratios than the Raman method (also see Table 1). The different values between the two methods could possibly be related to the sampling height. The transmission method could best be applied to, for example, features bound by clear sky at the higher heights where the signal attenuation is less and the molecular signal is still strong enough so that the method could produce results with less error.

For a fair comparison, the Raman and transmission methods were compared for ice cloud layers where the lidar ratios were derived from both methods. The ice cloud layers were further restricted to those with lidar ratio random errors below 30% for both the Raman and transmission method, which is the threshold for the best estimate lidar ratio (Thorsen & Fu, 2015). In addition, only ice cloud layers where the optical depth can be retrieved successfully from both methods are considered. For the comparison the lidar ratio from the Raman method was averaged vertically over the cloud layer. Figure 3 shows the resultant lidar ratio PDFs with the mean, median, and standard deviations listed in Table 3, indicating very similar results produced

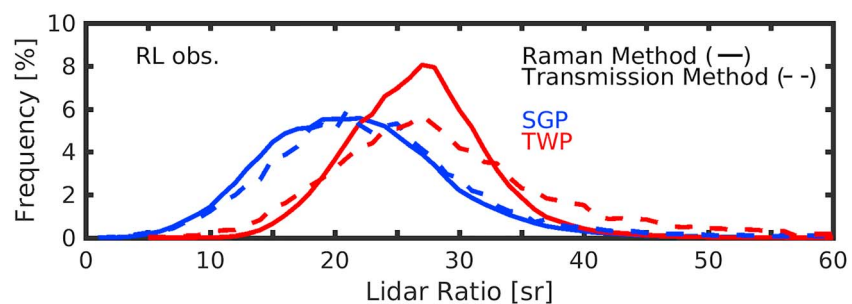


Figure 2. Probability distribution functions of ice cloud lidar ratio from the Raman method (solid) and transmission method (dashed) when used as the best estimate in the Raman lidar feature detection and extinction retrievals from August 2008 to August 2016 at the SGP site (blue) and December 2010 to January 2015 at the TWP site (red). SGP = Southern Great Plains; TWP = Tropical Western Pacific.

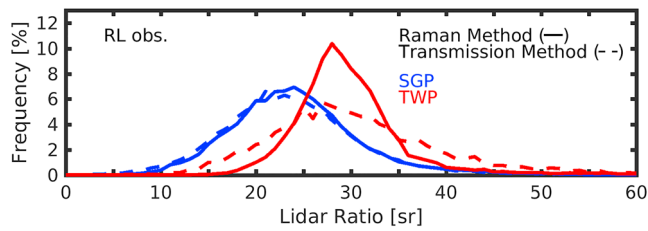


Figure 3. Probability distribution functions of cloud layer-averaged ice cloud lidar ratio for the Raman method (solid) and transmission method (dashed) for the same ice cloud layers observed by Raman lidars from August 2008 to August 2016 at the SGP site (blue) and December 2010 to January 2015 at the TWP site (red). SGP = Southern Great Plains; TWP = Tropical Western Pacific.

from the two methods. Overall, the Raman PDFs are narrower because of the larger temporal and spatial averaging involved in the method to enhance the SNRs (Thorsen & Fu, 2015). This narrowing of the PDFs is larger at TWP compared to SGP since high, very thin ice clouds are often observed in the tropical tropopause layer (Thorsen et al., 2011). The consistent lidar ratio statistics between Raman and transmission methods (Figure 3 and Table 3) allows us to use the results from either method for our analysis and comparisons to CALIPSO's retrievals.

It is noted that the RL FEX explicitly accounts for the multiple scattering effects in the retrieval (Thorsen & Fu, 2015) using a multiple scattering model (Hogan, 2006) to derive a function that describes the enhancement in the received signal caused by multiple scattering. Thorsen and Fu (2015) demonstrated the accuracy in their approach through comparisons

between the signals corrected for multiple scattering in the two RL fields of view (0.3 and 2 mrad). Furthermore, Thorsen and Fu (2015) show that these multiple scattering corrections are insensitive to the uncertainties in specifying the ice particle size and assumptions about the shape of near-backscatter phase function. This is further demonstrated in Appendix A where the ice particle size determined in this study following Heymsfield et al. (2014) is compared to the ice particle sizes used in Thorsen and Fu (2015; Figure A1). The updated ice particle sizes are much larger, leading to an increased multiple scattering effect but only resulting in a less than 3–9% change in the particulate extinction and lidar ratio and nearly identical particulate backscatter. Overall this provides confidence in our multiple scattering treatment and thus the errors in retrieved ice cloud lidar ratio and extinction due to the RL multiple scattering treatment are assumed to be small.

3. Relationship of Lidar Ratio and Temperature.

3.1. RL Observations

Radiosondes are launched up to 4 times daily from the ARM sites, and these temperature profiles are interpolated to match the RL FEX temporal and vertical resolution. Directly retrieved lidar ratios are matched with these temperatures and then binned every 2 K. Directly retrieved lidar ratios refer to retrievals using the Raman method, the transmission method, or measurements constrained by nearby Raman/transmission method retrieved features (interpolation; Thorsen & Fu, 2015). Directly retrieved lidar ratios comprise the first three methods (Raman, transmission, and interpolation) in Tables 1 and 2. Bins where the standard error is greater than 0.5 are removed (i.e., small sample sizes with large standard deviations). Median lidar ratio values for each bin are calculated and plotted in Figure 4 for SGP and TWP with the shaded region indicating the 25th to 75th percentile. Lidar ratios increase with temperature slightly when $T < 215$ (220) K but decrease with temperature when $T > 215$ (220) K at TWP (SGP) sites (Figure 4). Lidar ratios at TWP are higher than those at SGP but with a similar dependence on temperature. These results are consistent with Platt and Dille (1981) where they found that the lidar ratio overall decreased with cloud temperature. Gouveia et al. (2017) and Seifert et al. (2007) also showed little dependence of observed lidar ratio on temperature. Chen et al. (2002) showed an increase of lidar ratio with increasing cloud temperature for a similar temperature range (~200 to 230 K) in which the lidar ratio increased from

Table 3

Statistics of Lidar Ratios (Mean, Median, and Standard Deviation) in Units of sr for the Same Ice Cloud Layers Observed by RLS to Which Both the Raman and Transmission Methods Were Applied

Method	SGP			TWP		
	Mean	Median	Standard deviation	Mean	Median	Standard deviation
Raman	24.8	24.2	7.1	30.5	29.5	6.7
Transmission	24.4	23.7	8.1	31.3	29.8	9.9

Note. The numbers of ice cloud layers are 67,977 at the SGP site from August 2008 to August 2016 and 16,736 at the TWP site from December 2010 to January 2015. SGP = Southern Great Plains; TWP = Tropical Western Pacific.

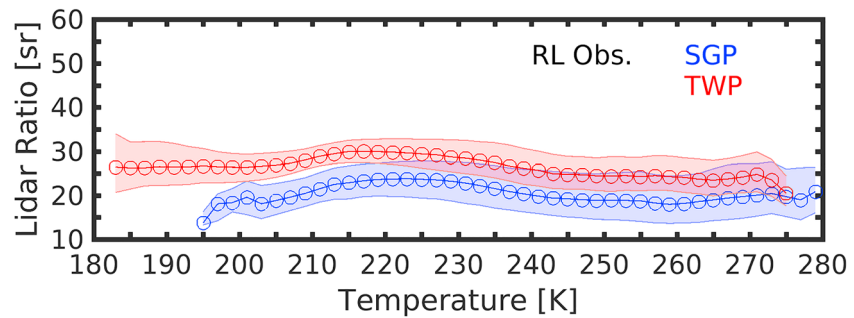


Figure 4. Median ice cloud lidar ratio binned by temperature in 2 K interval for all direct Raman lidar retrievals at the SGP (blue) site from August 2008 to August 2016 and at the TWP (red) site from December 2010 to January 2015. Shading corresponds to the 25th percentile through the 75th percentile. SGP = Southern Great Plains; TWP = Tropical Western Pacific.

the present RL observations. In contrast, Yorks et al. (2011) found decreases in lidar ratio with decreasing temperature for a larger range of temperatures (~200 to 270 K).

3.2. CALIPSO Observations

In the CALIPSO Version 4 data product, the ice cloud lidar ratio is parameterized as a function of cloud centroid temperature for unconstrained retrievals (Young et al., 2018). The parameterization is based on the cloud layer mean effective lidar ratio derived from the constrained retrievals for ice clouds bounded by clear air using the transmission method when it can be applied. The temperature dependence of the ice cloud lidar ratio is largely the result of the temperature-dependent multiple scattering factor implemented in CALIPSO's Version 4 data product (Garnier et al., 2015). Figure 5 compares the lidar ratios from the CALIPSO-constrained retrievals over the SGP and TWP sites with the lidar ratio parameterization as a function of temperature (Young et al., 2018). In Figure 5, the retrieved lidar ratios are binned by cloud centroid temperature for each 2 K bin and the median lidar ratio for each bin is plotted with the shaded region indicating the 25th to 75th percentiles. Bins with sample sizes below 15 or the 75th percentile larger than 100 sr were excluded. The median values from the constrained retrievals closely follow the parameterization, as expected since the parameterization was developed from constrained retrievals. The lidar ratios from the CALIPSO-constrained retrievals also show that the lidar ratios over the TWP site are higher than those over the SGP site, which is similar to the RL data.

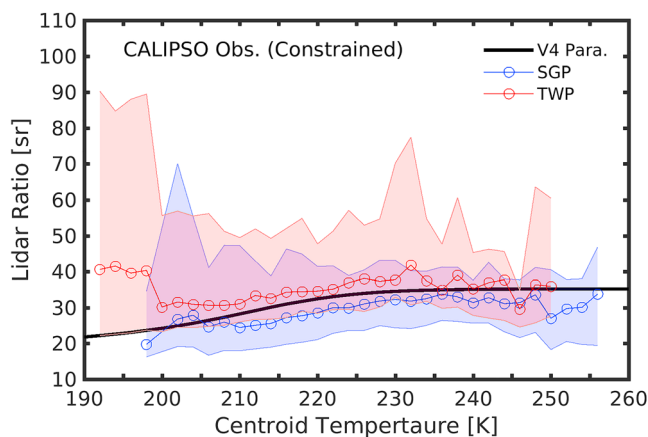


Figure 5. Median ice cloud layer mean lidar ratio binned by cloud centroid temperature in 2 K interval for all CALIPSO-constrained retrievals within 5° latitude by 5° longitude box centered over the SGP (blue) site and the TWP (red) site from June 2006 to August 2016. Shading corresponds to the 25th percentile through the 75th percentile. The CALIPSO Version 4 lidar ratio-cloud centroid temperature parameterization (black) is plotted for comparison. CALIPSO = Cloud-Aerosol Lidar and Infrared Pathfinder Satellite Observations; SGP = Southern Great Plains; TWP = Tropical Western Pacific.

The relationship between the cloud layer mean lidar ratio and cloud central temperature based on the RL and radiosonde data is constructed using both the best estimate observations from the Raman and transmission methods. Median values for each 2 K bin are plotted in Figures 6a and 6b for SGP and TWP, respectively, with the shaded region indicating the 25th to 75th percentiles. The mean temperatures for the observations of the best estimate Raman and transmission methods are 241.3 K (242.7 K) and 221.4 K (206.1 K) over SGP (TWP), respectively. As expected from the analysis in section 2.5 (Figure 3 and Table 3), little difference is seen in the lidar ratio-temperature relationships between the Raman and transmission methods based on the RL observations, in particular, for temperatures representative of SGP (~230 K) and TWP (~210 K). The lidar ratio-temperature relationships from the RL do not agree with the CALIPSO parameterization for SGP (Figure 6). For TWP, the CALIPSO parameterization falls within the 25th–75th percentile for the RL transmission method across the temperature range. Compared with the CALIPSO parameterization, little dependence of the lidar ratio on the cloud layer central temperatures is observed from the RL. The CALIPSO

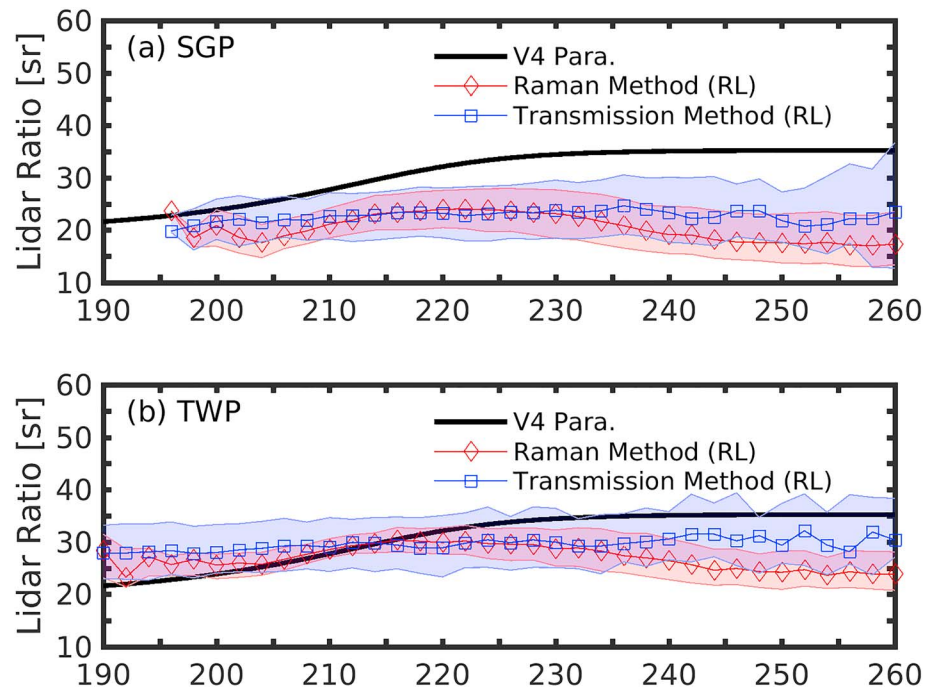


Figure 6. Median ice cloud layer mean lidar ratio binned by cloud layer central temperature in 2 K interval for the (a) SGP site from August 2008 to August 2016 and the (b) TWP site from December 2010 to January 2015. The results from the best estimate Raman lidar (RL) observations are separated into Raman (red diamond) and transmission (blue square) methods. Shading corresponds to the 25th percentile through the 75th percentile. The CALIPSO Version 4 lidar ratio-cloud centroid temperature parameterization (black) is plotted for comparison. CALIPSO = Cloud-Aerosol Lidar and Infrared Pathfinder Satellite Observations; SGP = Southern Great Plains; TWP = Tropical Western Pacific.

parameterization shows an increase of the lidar ratio with temperature, but the RL observations suggest an overall slight decrease with temperature, if any.

3.3. Relationship of Multiple Scattering Factor and Temperature

A new component of the ice cloud optical properties retrievals in the CALIPSO V4 is a new formulation of the ice cloud multiple scattering factor. In all data releases prior to V4, a constant of 0.6 was used for the ice cloud multiple scattering factor. In CALIPSO V4, the ice cloud multiple scattering factors decrease nonlinearly from ~ 0.8 to ~ 0.45 for increasing centroid temperatures (Young et al., 2018). The new parameterization of the CALIPSO multiple scattering factor is partly responsible for the temperature dependence seen in the CALIPSO V4 lidar ratios for ice clouds. Likewise, any errors in the temperature-dependent parameterization of the multiple scattering factor will be propagated into the corresponding lidar ratio retrievals (M. Vaughan, private communication, 2018). Therefore, to better understand the discrepancy in the lidar ratio's dependence on temperature, we assess the relationship of the CALIPSO multiple scattering factor and temperature for ice clouds using the best retrievals available from the RL and CALIPSO.

CALIPSO-constrained retrievals provide a measurement of the effective lidar ratio, that is, the product of the multiple scattering factor and the lidar ratio (Yang et al., 2010). In order to derive the lidar ratio from constrained retrievals, the multiple scattering factor must be assumed. For CALIPSO V4, the temperature-dependent parameterization of the multiple scattering factor is utilized to obtain the lidar ratio from constrained retrievals (Garnier et al., 2015). Here we use the effective lidar ratios from the CALIPSO V4 constrained retrievals and the best estimate transmission-retrieved lidar ratio from the RL observations, both are based on direct measurements without relying on a parameterization. RL observations with lidar ratios from the transmission method are considered because CALIPSO's constrained retrievals utilize the transmission method to retrieve the lidar ratio. By combining the constrained effective lidar ratio from CALIPSO observations with transmission-retrieved lidar ratio from RL observations binned by temperature, the multiple scattering factor relationship with temperature can then be estimated. The median value of the effective lidar ratio for constrained CALIPSO observations over SGP and TWP for each temperature bin is divided by all

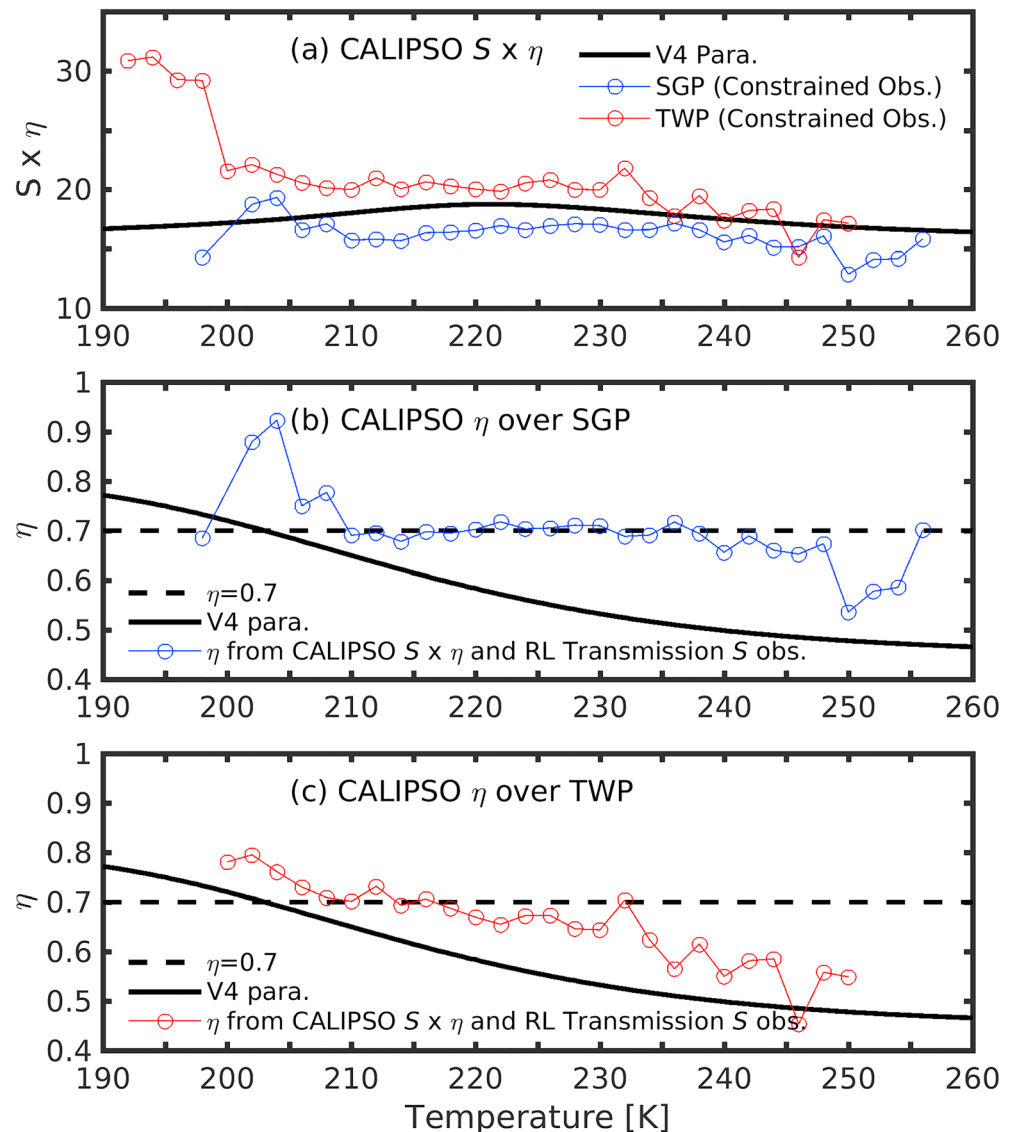


Figure 7. (a) Median effective lidar ratio binned by temperature in 2 K interval for all CALIPSO-constrained retrievals within 5° latitude by 5° longitude box centered over the SGP (blue) site and the TWP (red) site from June 2006 to August 2016. The CALIPSO Version 4 effective lidar ratio parameterization (i.e., the product of the multiple scattering factor and lidar ratio based on the CALIPSO V4 temperature-dependent parameterizations) is plotted for comparison (solid black). Median multiple scattering factor binned by temperature in 2 K interval for median effective lidar ratio divided by best estimate transmission-retrieved RL observations for the (b) SGP site from August 2008 to August 2016 and the (c) TWP site from December 2010 to January 2015. The CALIPSO Version 4 temperature-dependent multiple scattering factor (solid black) and constant multiple scattering factor of 0.7 (dashed black) are plotted for comparison. RL = Raman lidar; CALIPSO = Cloud-Aerosol Lidar and Infrared Pathfinder Satellite Observations; SGP = Southern Great Plains; TWP = Tropical Western Pacific.

the transmission-retrieved lidar ratios from RL observations for SGP and TWP in the corresponding temperature bin. This yields the CALIPSO multiple scattering factor as a function of temperature implied by the RL-retrieved lidar ratios. Transmission-retrieved RL observations here are limited to those from profiles that have ice cloud column optical depths within the middle 95% of CALIPSO ice cloud column optical depth distribution ($6.6E-3$ to 2.3 for SGP and $6.5E-3$ to 2.0 for TWP). Figure 7a shows the median effective lidar ratio from CALIPSO-constrained observations over SGP and TWP for 2 K bin along with the effective lidar ratio derived from the CALIPSO temperature-dependence parameterizations of the multiple scattering factor and lidar ratio for a comparison. The effective lidar ratio based on the

parameterizations is between the observed effective lidar ratios over the SGP and TWP sites. The median multiple scattering factors from combining CALIPSO-constrained effective lidar ratio observations and RL transmission-retrieved lidar ratio observations are plotted for 2 K bin for SGP in Figure 7b and for TWP in Figure 7c. The CALIPSO parameterization of the multiple scattering factor is also plotted in Figures 7b and 7c for a comparison. The resultant multiple scattering factor for temperatures representative of ice clouds at SGP (~230 K) and TWP (~210 K) are both approximately 0.7 with small variations across changes in temperature. Overall, the median multiple scattering factor is 0.70 (0.67) with a standard deviation of 0.07 (0.08) for SGP (TWP). We conclude that the CALIPSO multiple scattering factors derived using constrained effective lidar ratio from the CALIPSO observations and transmission-retrieved lidar ratio from the RL observations (i.e., ~0.7 for both SGP and TWP) do not support the temperature-dependent parameterization of the multiple scattering factor used in the CALIPSO V4.

4. Effects of Lidar Ratio and Sampling Resolution (Averaging) on Retrieved Optical Depth

Only ice cloud column optical depths of RL transparent profiles are analyzed in this section. The impacts on ice cloud column optical depth distributions by the lidar ratio are assessed in section 4.1 and by resolution in section 4.2.

4.1. Lidar Ratio Effect

The ice cloud column optical depth can be derived with the lidar ratio and particulate backscatter from the RL observations in the form of

$$\tau_{i,c} = \int_{z_{\text{base}}}^{z_{\text{top}}} S(z)\beta_i(z)dz, \quad (3)$$

where β_i is ice cloud particulate backscatter, S is the lidar ratio, and z_{top} (z_{base}) is the highest (lowest) ice cloud top (base) height of the atmospheric profile.

RL FEX retrieves the ice cloud lidar ratios (section 2.5), which along with those employed in the CALIPSO V4 are used in equation (3) to examine how the lidar ratio impacts the retrieved ice cloud optical depth based on the RL observations. For this purpose, ice cloud column optical depths of transparent profiles are retrieved by using three sets of lidar ratios: (1) best estimate from the RL FEX (Thorsen & Fu, 2015; also, see section 2.1 for the update); (2) the CALIPSO V4 temperature-dependent lidar ratio parameterization, and (3) the effective lidar ratio determined by the CALIPSO V4 temperature-dependence parameterizations of the multiple scattering factor and lidar ratio (i.e., the solid line in Figure 7a), divided by a constant multiple scattering factor of 0.7. The lidar ratio from the third set is consistent with both CALIPSO-observed effective lidar ratio and RL-observed lidar ratio, which is thus very similar to that used in the first set. The third set will also be used in the CALIPSO ice cloud column optical depth retrievals to compare with those using the CALIPSO default lidar ratio parameterizations (i.e., the second set) in section 5. The temperature for transparent ice clouds have a mean of 228.1 K (207.0 K) for SGP (TWP). The lidar ratios following the CALIPSO V4 parameterization for transparent ice clouds has a mean of 32.8 sr (26.5 sr) for SGP (TWP). The lidar ratios following the CALIPSO V4 parameterization of effective lidar ratio divided by a constant multiple scattering factor of 0.7 for transparent ice clouds have a mean of 25.8 sr (24.9 sr) for SGP (TWP). For a comparison, the mean lidar ratio from the RL best estimate for the transparent profiles is 23.1 sr (28.6 sr) over SGP (TWP; Table 2). The small differences within $\sim \pm 10\%$ in the mean lidar ratios between the third and first sets are because the CALIPSO effective lidar ratio based on the parameterizations is slightly larger (smaller) than the observations over SGP (TWP; see Figure 7a).

The ice cloud column optical depths for transparent ice cloudy profiles with different lidar ratios are plotted in Figure 8 as cumulative distribution functions (CDFs). For SGP, the different lidar ratios shifts the ice cloud column optical depth distribution to higher optical depths relative to the best estimate. Most notably, the CALIPSO V4 temperature-dependent parameterization of lidar ratio shifts the distribution to much larger optical depths, increasing the mean ice cloud column optical depth by 57% from 0.28 to 0.44. The CALIPSO V4 effective lidar ratio based on the parameterizations divided by a constant multiple scattering factor of 0.7 shifts the optical depth distribution and mean to slightly larger values because of a slight overestimation of the effective lidar ratio based on the parameterizations (Figure 7a).

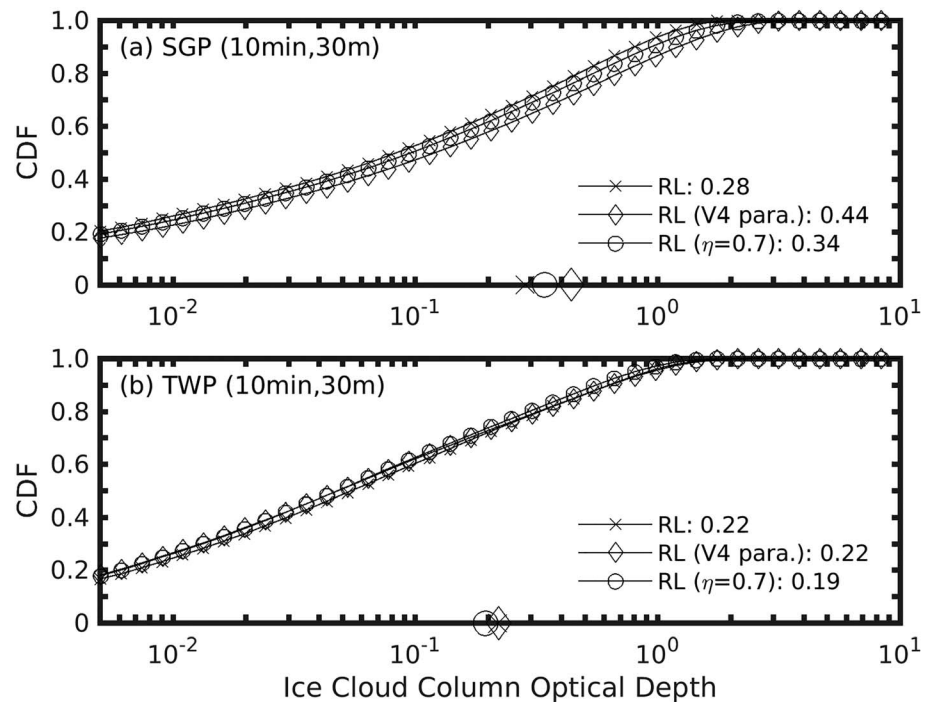


Figure 8. Cumulative distribution functions (CDFs) of ice cloud column optical depths from the RLs using different lidar ratios for transparent ice cloudy profiles at the (a) SGP site from August 2008 to August 2016 and at the (b) TWP site from December 2010 to January 2015. The FEX-retrieved extinction (“x”) based on the best estimate lidar ratio. The CALIPSO Version 4 temperature-dependent lidar ratio parameterization (‘◇’) that is used in CALIPSO version 4 for unconstrained ice cloud retrievals. The CALIPSO Version 4 effective lidar ratio parameterization that is used in CALIPSO Version 4 for unconstrained ice cloud retrievals divided by a constant multiple scattering factor of 0.7 (‘○’). Mean values are plotted on the bottom of the graphs and labeled in the legend as well. FEX = feature detection and extinction; RL = Raman lidar; CALIPSO = Cloud-Aerosol Lidar and Infrared Pathfinder Satellite Observations; SGP = Southern Great Plains; TWP = Tropical Western Pacific.

For TWP, the ice cloud column optical depth distributions are less affected by the choice of lidar ratios. The CALIPSO V4 parameterization of lidar ratio overall leads to little shift, which is a result of the competing balance between the RL lidar ratios exceeding the parameterization at lower temperatures and those below the parameterization at higher temperatures (Figure 6). This interpretation is supported by the fact that the mean column ice cloud temperature for transparent profiles weighted by column optical depth at TWP is 211 K, which is near the point where the RL data switch from exceeding the parameterization to falling below the parameterization (Figure 6). The CALIPSO V4 effective lidar ratio parameterization divided by a constant multiple scattering factor of 0.7 shifts the optical depth distribution and mean to slightly smaller values since the derived mean lidar ratio is less than the RL best estimate.

4.2. Resolution (Averaging) Effects

The identification of transparent profiles for the RL somewhat depends on the amount of averaging used. With increased averaging, either temporally or vertically, the SNR increases. Therefore, the ability to exceed the transparent threshold of $SNR > 1$ at 16 km at SGP and 18 km at TWP increases with increasing temporal and vertical averaging. Optically thin targets also benefit from increased averaging for detection purposes (e.g., Winker et al., 2010). Conversely, features can be smeared out with increased averaging so that less structure is captured compared to higher resolutions as noted by Thorsen et al. (2015). To understand the implications on ice cloud column optical depths, RL FEX was run at several different temporal and vertical resolutions. The resolutions examined include (1) 10 min/30 m, (2) 10 min/60 m, and (3) 8 min/60 m for SGP and 24 min/60 m for TWP. The first (10 min/30 m) is the nominal resolution used in this study. The vertical resolution (averaging) of 60 m matches that for CALIPSO above 8.2 km, where most ice clouds are found. The 8- and 24-min temporal resolutions are found to best represent the CALIPSO-like resolutions in extinction retrievals over SGP and TWP, respectively (see section 5).

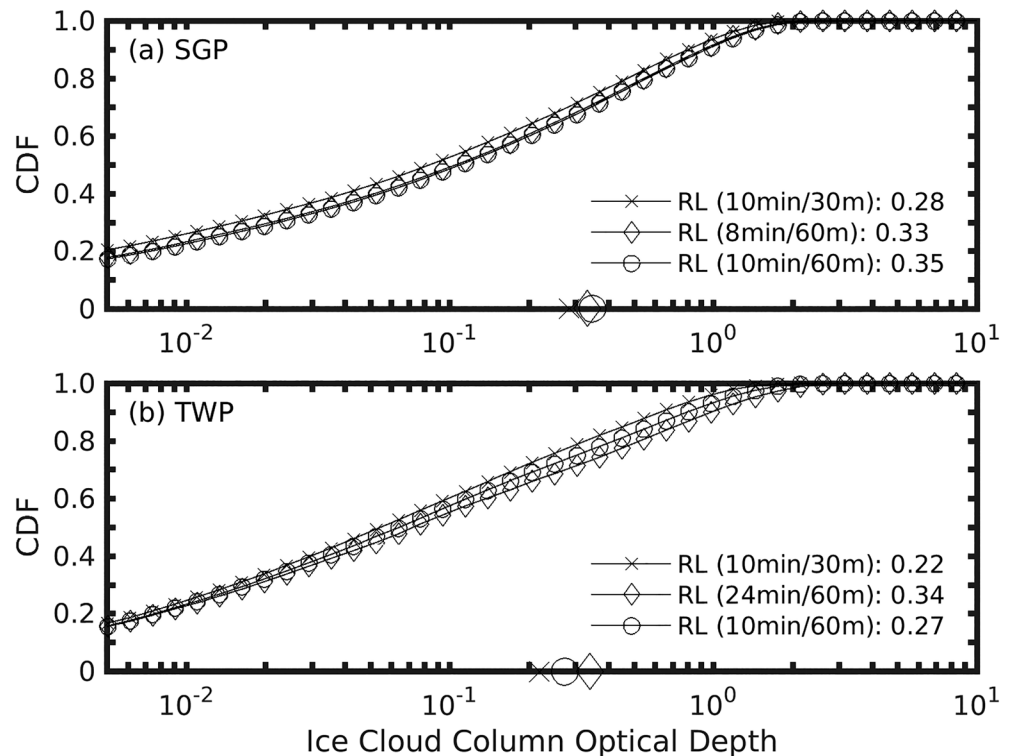


Figure 9. Cumulative distribution functions (CDFs) of ice cloud column optical depth retrieved from the RL observations with temporal and vertical resolution of 10 min/30 m (“x”), 10 min/60 m (“o”), and 8 min/60 m (“◊”) for SGP, and 24 min/60 m (“◊”) for TWP for transparent ice cloudy profiles at the (a) SGP site from August 2008 to August 2016 and at the (b) TWP site from December 2010 to January 2015. Mean values are plotted on the bottom of the graphs and labeled in the legend as well. RL = Raman lidar; SGP = Southern Great Plains; TWP = Tropical Western Pacific.

The CDFs of ice cloud column optical depths for ice cloudy transparent profiles with different resolutions are plotted in Figure 9 for both sites. At SGP, the 10-min/30-m resolution, which has the lowest mean value, exceeds 90% cumulative distribution at an optical depth of 0.88 as compared to 1.00–1.03 for the other distributions. The 10-min/60-m resolution contains higher optical depth values and also has the highest mean optical depth of 0.35. For a constant temporal resolution of 10 min, the change in vertical resolution from 30 to 60 m resulted in a 25% increase in the mean ice cloud column optical from 0.28 to 0.35. At TWP, similar patterns are noted. However, resolution plays a larger role in affecting the ice cloud column optical depth distribution at TWP than at SGP. The 10-min/30-m resolution exceeds 90% cumulative distribution at a lower optical depth and the increase in the mean from 10 min/30 m to 24 min/60 m is 55% from 0.22 to 0.34. Comparing the resolution change between SGP and TWP for the resolution that best matches CALIPSO’s extinction retrieval, the increase in the mean at TWP (55%) is more than double the relative change at SGP (18%). Ice cloud column optical depth distributions from the RLs contained higher optical depths by increasing temporal and vertical averaging. This is because an increase in averaging of the signal enhances the likelihood of satisfying the transparent definition of $SNR > 1$. Therefore, decreased temporal and vertical resolution (i.e., increased averaging) allows larger ice cloud column optical depths to be classified as transparent profiles.

5. Comparison of RL and CALIPSO Ice Cloud Observations

In this section we first determine the temporal resolution (averaging) for the RL observations to be consistent with the CALIPSO observations and then carry out the comparison. The fairest comparison would be to pair the resolution that matches the SNR since this term ultimately determines if the instrument can detect clouds. Here we have chosen to match the RL and CALIPSO resolution based on the horizontal wind speed and averaging distance. This is because the SNRs are dependent on instrument specifications that we cannot completely account for in a comparison of retrieved quantities. Any resultant differences could partly

be a result of this, and we will later examine the role of instrument sensitivity and the transparent definition for this comparison.

5.1. Determining CALIPSO-Like Resolution

A fair comparison of the RL and CALIPSO necessitates sampling the atmosphere with comparable resolutions. We use the RL FEX data with a vertical resolution of 60 m to match CALIPSO's cloud product resolution from 8.2 to 20.2 km. The altitude range corresponds to the heights where ice clouds typically form (Heymans et al., 2017).

Matching temporal resolutions requires quantifying how much of the atmosphere is typically sampled by CALIPSO's horizontal averaging. CALIPSO's data product identifies features using an algorithm called the selective iterative boundary locator detailed in Vaughan et al. (2009). The selective iterative boundary locator detects features at five horizontal resolutions: 1/3, 1, 5, 20, and 80 km. For extinction retrievals, only layers detected at 5-, 20-, and 80-km horizontal averaging resolution are used because SNR are often too low for reliable extinction retrievals at 1/3 and 1 km. Therefore, one matching temporal resolution will be constructed for feature detection and another matching temporal resolution will be constructed for extinction retrievals.

CALIPSO mean horizontal averaging distance profiles for feature detection and extinction retrievals are first derived for collocated transparent ice clouds over SGP (Figure 10a) and TWP (Figure 10b). Mean wind speed profiles are obtained from the collocated radiosondes at SGP (Figure 10a) and TWP (Figure 10b). These mean horizontal averages are divided by the horizontal wind speed as the atmosphere is advected over the ground-based instrument to obtain the equivalent averaging period for a ground-based instrument (Figure 10c).

An ice cloud occurrence-weighted vertical average of the equivalent temporal resolution profiles for both feature detection and extinction retrievals are obtained using CALIPSO's ice cloud occurrence profile. For feature detection, this yields 5.9 min at SGP and 19.9 min at TWP. For extinction retrievals, this yields 8.0 min at SGP and 25.6 min at TWP. Therefore, we take the RL temporal resolutions of 5 min for SGP and 20 min for TWP as the feature detection CALIPSO-like, and 8 min for SGP and 24 min for TWP as the extinction retrieval CALIPSO-like (denoted by the vertical lines in Figure 10c). A resolution of 24 min is used for TWP because it allows no incomplete time steps over 1 day for the daily-based RL FEX retrieval scheme. For the collocated profiles using the feature detection CALIPSO-like resolution, 68% and 67% of the RL observations were transparent at SGP and TWP, respectively. For the collocated profiles using the extinction retrieval CALIPSO-like resolution, 69% and 68% of the RL observations were transparent at SGP and TWP, respectively. Recall that 68% (SGP) and 60% (TWP) of the collocated RL observations were transparent with 10-min/30-m resolutions (see section 2.3). The percentage of collocated RL profiles at the CALIPSO-like resolutions that are transparent are higher than those found for CALIPSO in section 2.3 (i.e., 60% for SGP and 55% and TWP).

5.2. Cloud Occurrence Comparison

Ice cloud fractions are calculated using the transparent collocated profiles (see section 2.3) for the comparison. Cloud fraction is defined as the number of profiles where ice clouds are detected divided by the total number of available transparent collocated profiles. Cloud fractions were separated into all profiles, nighttime-only profiles, and daytime-only profiles. Splitting into nighttime and daytime helps to separate the impacts of solar background contamination on the results. The RL-only analysis in section 4 was not separated into daytime and nighttime since solar background contamination has a small effect on cloud detection with the RL (Thorsen et al., 2013).

Cloud fractions are listed in Table 4 for CALIPSO and the RLs. The RL results are shown with resolution of 10 min/30 m and with feature detection CALIPSO-like resolutions of 5 min/60 m at SGP and 20 min/60 m at TWP. The RL observes more ice cloudy profiles than CALIPSO at both SGP and TWP sites for both averaging amounts. The RL with the CALIPSO-like temporal resolution of 5 min/60 m at SGP agrees more with CALIPSO than the RL with averaging of 10 min/30 m. But at TWP, the RL with the CALIPSO-like resolution of 20 min/60 m agrees less with CALIPSO than the RL with 10-min/30-m averaging. Nighttime cloud fractions are higher than daytime cloud fractions for both observations, but the difference is larger for CALIPSO. CALIPSO's sensitivity is reduced during the daytime when solar background contamination is prevalent,

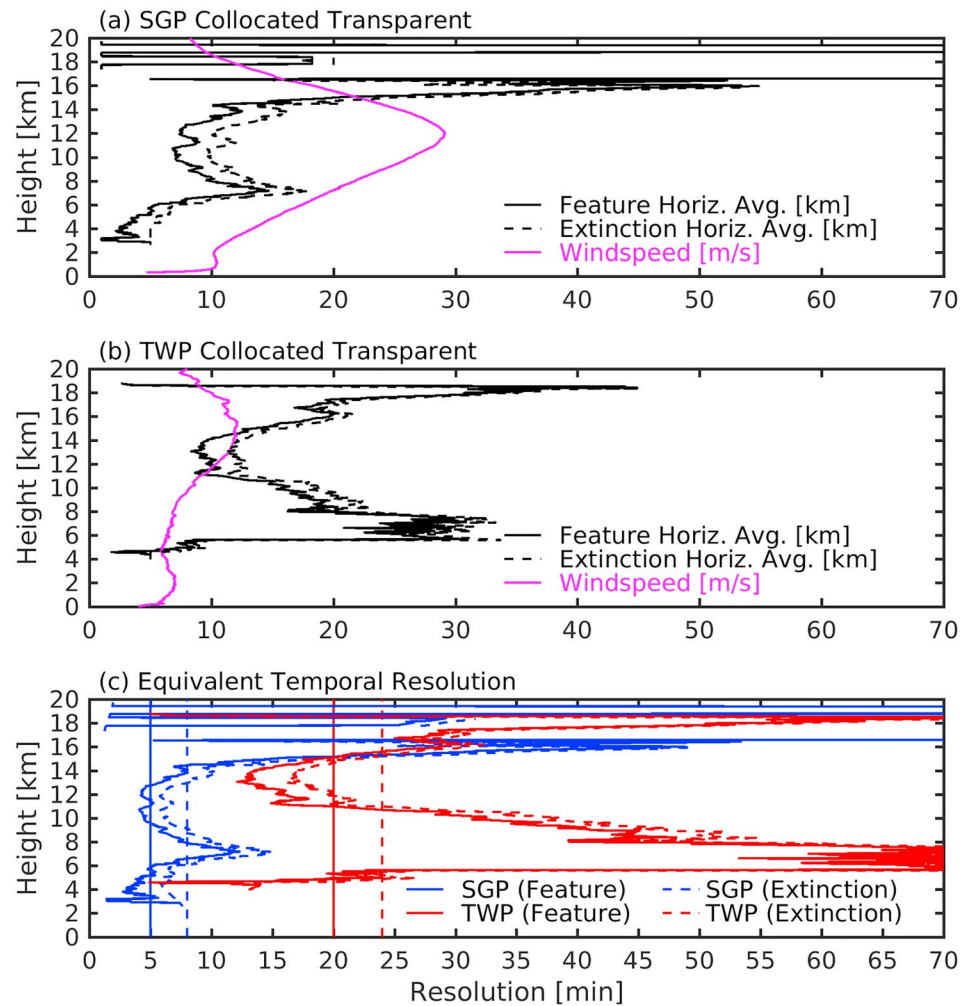


Figure 10. Mean wind profile (pink) from collocated radiosonde data and CALIPSO mean horizontal averaging distance profile (black) from CALIPSO's feature detection (solid) and CALIPSO's extinction retrievals (dashed) for collocated transparent ice clouds at the (a) SGP site from August 2008 to August 2016 and at the (b) TWP site from December 2010 to January 2015. Dividing the mean horizontal averaging distance by the mean wind yields the (c) equivalent temporal resolution profile for SGP (blue) and TWP (red) matched to CALIPSO's feature detection (solid) and CALIPSO's extinction retrievals (dashed) with corresponding reference lines for 5, 8, 20, and 24 minutes. CALIPSO = Cloud-Aerosol Lidar and Infrared Pathfinder Satellite Observations; SGP = Southern Great Plains; TWP = Tropical Western Pacific.

which is less of a concern for the RL. But it is not clear whether the difference in the cloud fraction between daytime and nighttime from RL is real or still partly related to the solar contamination. Furthermore, as will be seen in section 5.3, the significantly larger cloud fraction from RL than CALIPSO (Table 4) is a result of a much higher sensitivity of RL to detect optically very thin ice clouds. The transparent collocated CALIPSO and RL data are used to construct cloud occurrence profiles, defined as the number of ice clouds detected at a given height divided by the total number of available profiles for each height. Cloud occurrence profiles are plotted in Figure 11 for CALIPSO, and the RL with resolutions of 10 min/30 m, and feature detection CALIPSO-like resolutions of 5 min/60 m at SGP and 20 min/60 m at TWP. The cloud occurrence profiles including both day and night (Figures 11a and 11b) show a general agreement between the RL and CALIPSO. With the CALIPSO-like resolution, more clouds are observed by the RL than CALIPSO at and below maximum ice cloud occurrence height near 15 km at TWP. With the feature detection CALIPSO-like resolutions, the nighttime profiles (Figures 11c and 11d) indicate that CALIPSO detects more ice clouds at SGP around 11 km but less below 6.5 km in contrast to the overall good agreement at TWP throughout the profile. The daytime profiles (Figures 11e and 11f) highlight more ice clouds detected by the RL compared to CALIPSO for all heights at SGP. Similarly, the RL detects more ice clouds than

Table 4

Cloud Fraction of Transparent Collocated Profiles for Both Day and Night (All), Nighttime Only (N), Daytime Only (D), From RL With 10-min/30-m Resolution and Feature Detection CALIPSO-Like Resolutions (i.e., 5 min/60 m at SGP and 20 min/60 m at TWP), and Cloud Fraction From the CALIPSO Product

Measurement	CF (All)	CF (N)	CF (D)
		SGP	
RL (10 min, 30 m)	0.37	0.39	0.35
RL (5 min, 60 m)	0.33	0.34	0.32
CALIPSO	0.24	0.28	0.20
		TWP	
RL (10 min, 30 m)	0.67	0.71	0.59
RL (20 min, 60 m)	0.73	0.76	0.66
CALIPSO	0.57	0.62	0.49

Note. RL = Raman lidar; CALIPSO = Cloud-Aerosol Lidar and Infrared Pathfinder Satellite Observations; SGP = Southern Great Plains; TWP = Tropical Western Pacific.

CALIPSO at TWP, especially with the feature detection CALIPSO-like resolution. Overall, the RL detects more ice clouds than CALIPSO when looking at each vertical height level for daytime profiles, and a closer agreement is found between the RL and CALIPSO for nighttime profiles when the influence of solar background noise is not present.

5.3. Ice Cloud Column Optical Depth Comparison

Ice cloud column optical depths from the RLs and CALIPSO are compared for transparent collocated ice cloudy profiles. The RL ice cloud column optical depths are expressed in equations (1) and (3). CALIPSO's ice cloud column optical depths are also computed with equation (1) using the CALIPSO cloud profile data set. The impact of different lidar ratios and multiple scattering factors on the CALIPSO ice cloud column optical depth is assessed by using the effective lidar ratio determined by the CALIPSO V4 temperature-dependent parameterizations of the multiple scattering factor and lidar ratio, divided by a constant multiple scattering factor of 0.7 (see section 3.3). These lidar ratios and multiple scattering factors

are then consistent with the RL transmission-retrieved lidar ratio and CALIPSO-constrained retrievals of effective lidar ratios. All CALIPSO-collocated transparent profiles are considered. Following Yang et al. (2010) (see their equation (4)), the CALIPSO ice cloud column optical depths with the constant multiple scattering factors are constructed as

$$\tau_{i,c}' = \int_{z_{\text{base}}}^{z_{\text{top}}} \frac{\alpha_i(z)\eta_T(z)}{\eta'} dz, \quad (4)$$

where α_i is the CALIPSO ice cloud particulate extinction, η_T is the CALIPSO temperature-dependent multiple scattering factor parameterization in version 4, and η' is a constant multiple scattering factor of 0.7. Note that using these constant multiple scattering factors also changes the lidar ratio but keeps the effective lidar ratio the same.

5.3.1. Cumulative Distribution Functions of Ice Cloud Column Optical Depth for Ice Cloudy Conditions

The cumulative distribution functions (CDFs) of ice cloud column optical depths for transparent collocated ice cloudy profiles are plotted in Figure 12 for CALIPSO, and RL with the nominal resolution (i.e., 10 min/30 m) and the extinction retrieval CALIPSO-like resolutions (i.e., 8 min/60 m at SGP and 24 min/60 m at TWP). The CDFs of ice cloud column optical depths retrieved from the RL using the CALIPSO temperature-dependent lidar ratio parameterization and the CALIPSO effective lidar ratio parameterization divided by a constant multiple scattering factor of 0.7 with the extinction retrieval CALIPSO-like resolutions are also plotted in Figure 12 for the comparison. The CDFs of ice cloud column optical depths retrieved from the CALIPSO using the CALIPSO effective lidar ratio parameterization and a constant multiple scattering factor of 0.7 (i.e., equation (4)) are also plotted in Figure 12 to examine the impact of the CALIPSO multiple scattering factor treatment for given effective lidar ratio. It is noted again that the use of the CALIPSO V4 effective lidar ratio along with a constant CALIPSO multiple scattering factor of 0.7 led to a lidar ratio that is largely consistent with the RL transmission-retrieved lidar ratios. The horizontal axis in Figure 12 is for optical depth with a logarithmic scale from 0.005 to 10. The CDFs are presented for all times (upper panel), nighttime only (middle panel), and daytime only (lower panel) over SGP (left panel) and TWP (right panel). The CALIPSO ice cloud column optical depths are larger than the RL ice cloud column optical depth in mean values except when the RL uses the equivalent averaging to the CALIPSO and the RL and CALIPSO use the same lidar ratio (as that used by either CALIPSO or the RL). The CDFs of the RL and CALIPSO are closer together for τ larger than about 0.3, which is particularly true for the RL when using the same averaging and the same lidar ratio. However, disagreement is observed for thinner optical depths. Figure 12 suggests that the RL sensitivity is much higher than CALIPSO for detecting optically very thin ice clouds. These results are consistent with Davis et al. (2010) who found that when comparing CALIPSO with an aircraft lidar that CALIPSO is insensitive to optically very thin clouds. The disagreement for thinner optical depths but similar mean ice cloud column optical depth when using consistent lidar ratios and resolution

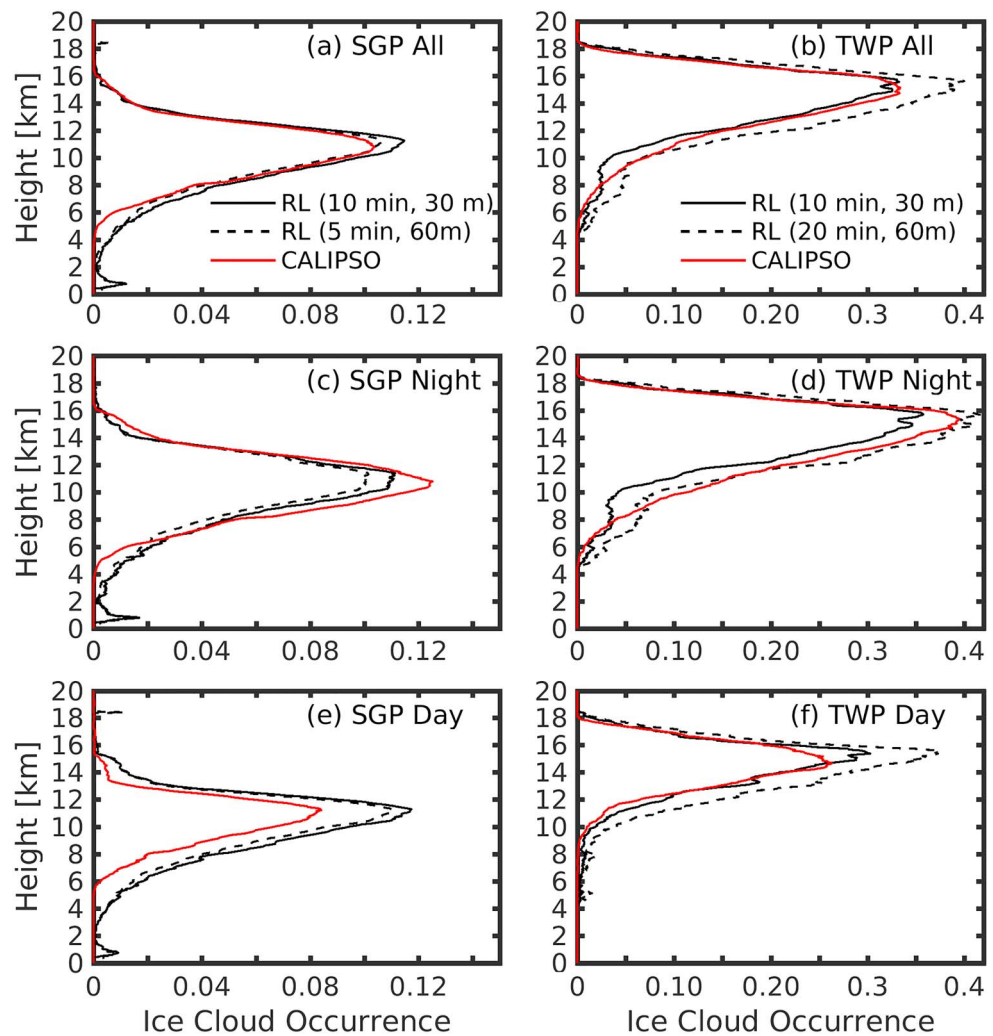


Figure 11. Ice cloud occurrence profiles from CALIPSO (red) and RL with 10-min/30-m resolution (solid black) and feature detection CALIPSO-like resolutions (i.e., 5 min/60 m for SGP and 20 min/60 m for TWP) (dashed lines). Only transparent collocated profiles are considered. Panels (a) and (b) for profiles from both day and night, (c) and (d) for night time only, and (e) and (f) for day time only, with SGP on the left (a, c, and e) from August 2008 to August 2016 and TWP on the right (b, d, and f) from December 2010 to January 2015. RL = Raman lidar; CALIPSO = Cloud-Aerosol Lidar and Infrared Pathfinder Satellite Observations; SGP = Southern Great Plains; TWP = Tropical Western Pacific.

suggests that the higher optical depths are larger for the RL than CALIPSO. This is supported by the fact that the mean of ice cloud column optical depths above 0.3 after accounting for the lidar ratio and resolution differences is 0.75 (0.81) for CALIPSO and 0.92 (0.97) for the RL at SGP (TWP).

For CALIPSO, significantly larger mean ice cloud column optical depths are observed during the nighttime than those during daytime. This is at least in part because of the lower daytime SNR, although other physical or artificial sources may exist. For the RL, larger mean ice cloud column optical depths are also observed during the nighttime than the daytime, especially over TWP.

Comparing results in Figures 12a and 12b with those in Figure 1, the difference at the SGP (TWP) site shown in Figure 1 is related to the lidar ratio and the resolution. Note that for a given CALIPSO effective lidar ratio, the multiple scattering factor and lidar ratio are not independent of each other (i.e., one can be derived from the other). Figure 12 indicates that the relative differences in ice cloud column optical depth are more due to the lidar ratio than averaging resolution at SGP but vice versa at TWP. The remaining large differences in the CDF for the lower optical depths will be discussed in the next subsection.

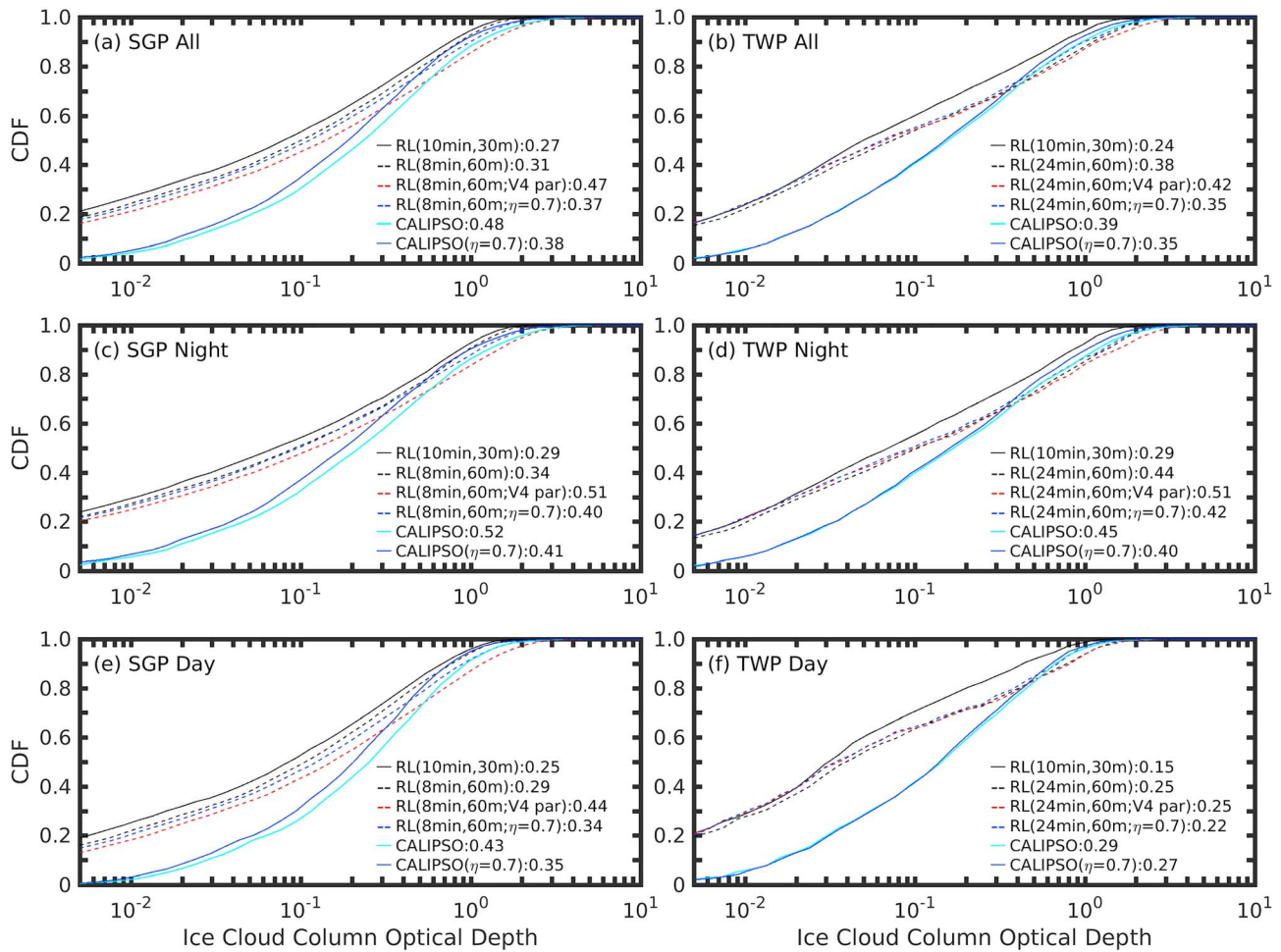


Figure 12. Cumulative distribution functions (CDFs) of ice cloud column optical depth for transparent collocated ice cloudy profiles from Cloud-Aerosol Lidar and Infrared Pathfinder Satellite Observations (CALIPSO) (cyan), CALIPSO using the CALIPSO V4 effective lidar ratio parameterization with a constant multiple scattering factor of 0.7 (blue), the Raman lidar (RL) with 10-min/30-m resolution using the best estimate lidar ratios (solid black), and the RL with extinction retrieval CALIPSO-like resolutions (i.e., 8 min/60 m at Southern Great Plains, SGP, and 24 min/60 m at Tropical Western Pacific, TWP) using the best estimate lidar ratios (black dashed) and those determined by the CALIPSO's Version 4 temperature-dependent lidar ratio parameterization (red dashed) and CALIPSO's Version 4 effective lidar ratio divided by a constant multiple scattering factor of 0.7 (blue dashed). SGP corresponds to the left side of the panel and TWP to the right side with all profiles on top (a and b), nighttime only profiles in the middle (c and d), and daytime only profiles on the bottom (e and f). Mean values are labeled in the legend. Data are for times collocated between the RL and CALIPSO at the SGP site from August 2008 to August 2016 and the TWP site from December 2010 to January 2015.

5.3.2. CDFs of Ice Cloud Column Optical Depth for All-Sky Conditions

The CDFs of the RL and CALIPSO ice cloud column optical depths are compared for all-sky conditions; that is, both ice cloudy profiles and profiles with $\tau_{i,c} = 0$, are now considered. These all-sky conditions are more relevant to the radiative effect of ice clouds. To demonstrate the motivation of this analysis, consider a simplistic example in which the CALIPSO's mean ice cloud column optical depth is 0.1 for ice cloudy profiles with an ice cloud fraction of 0.3 and the RL's mean ice cloud column optical depth is also 0.1 for the same ice cloudy profiles with the same ice cloud fraction as CALIPSO. But because of the high sensitivity, RL detects additional ice cloudy profiles with a cloud fraction of 0.4 with a mean ice cloud column optical depth of 0.005. Therefore, in ice cloudy conditions, the mean ice cloud column optical depths are 0.1 for CALIPSO and 0.0457 for RL. However, when including all transparent collocated profiles (i.e., $\tau_{i,c} = 0$ and $\tau_{i,c} > 0$), CALIPSO's all-sky mean becomes 0.03 and RL's all-sky mean becomes 0.032. The agreement for the all-sky means takes into account the differences in instrument sensitivity by considering the cloud fraction through incorporating all transparent collocated profiles in addition to the ice cloud column optical depth.

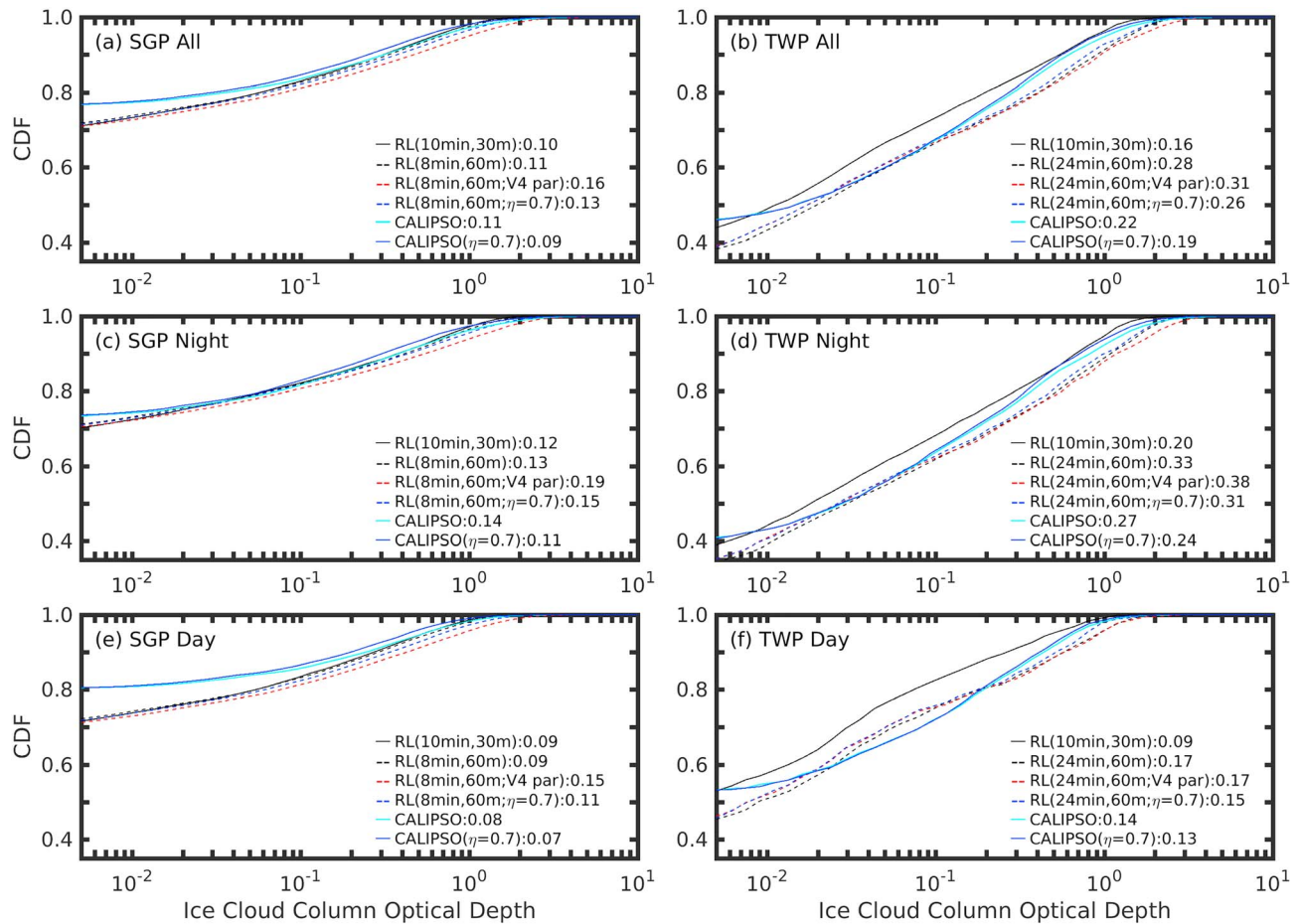


Figure 13. The same as Figure 12 but for all the transparent collocated profiles including both ice cloudy and clear profiles.

CDFs of transparent collocated ice cloud column optical depths under all-sky conditions are plotted in Figure 13 for CALIPSO and the RL. The RL and CALIPSO CDFs agree well, which is particularly true when the RL uses a resolution and lidar ratio consistent with the CALIPSO. A much better agreement between the CALIPSO and the RL CDFs is seen for lower optical depth in Figure 13 than in Figure 12, where only ice cloud profiles are considered. This is caused by CALIPSO's lower cloud fractions combined with its larger optically thick ice clouds as compared to the RL's higher cloud fractions with more optically thin ice clouds. However, the mean all-sky ice cloud column optical depth for the RLs are larger than those for CALIPSO.

CDFs of ice cloud column optical depths for all transparent collocated profiles including those with $\tau_{i,c} = 0$ are plotted in Figures 13c and 13d for nighttime only and in Figures 13e and 13f for daytime only. For nighttime-only profiles, similar good agreement is found at both SGP and TWP between the RL and CALIPSO ice cloud column optical distributions when comparable resolution and lidar ratio are used. For daytime only profiles, good agreement is also observed at both SGP and TWP between the RL and CALIPSO. Similar to the results by considering all profiles, both nighttime-only and daytime-only profiles observed smaller all-sky mean ice cloud column optical depths from CALIPSO than those from the RL.

5.3.3. Impact of Using More Consistent Transparent Profiles Between RL and CALIPSO

We define the transparent profiles differently for CALIPSO and RL (section 2.3) which may cause differences in the ice clouds sampled between the two data sets. Here we force more consistent transparent profiles between CALIPSO and RL. For this purpose, the percentages of transparent profiles (i.e., the number of transparent collocated profiles divided by the total number of collocated profiles) are first determined for both CALIPSO and RL observations for each collocated flyover section. Here a collocated flyover section refers to all RL profiles within ± 4 hr for a given single CALIPSO flyover time and all CALIPSO profiles within 5° latitude by 5° longitude box centered over SGP or TWP for the same flyover time. Transparent

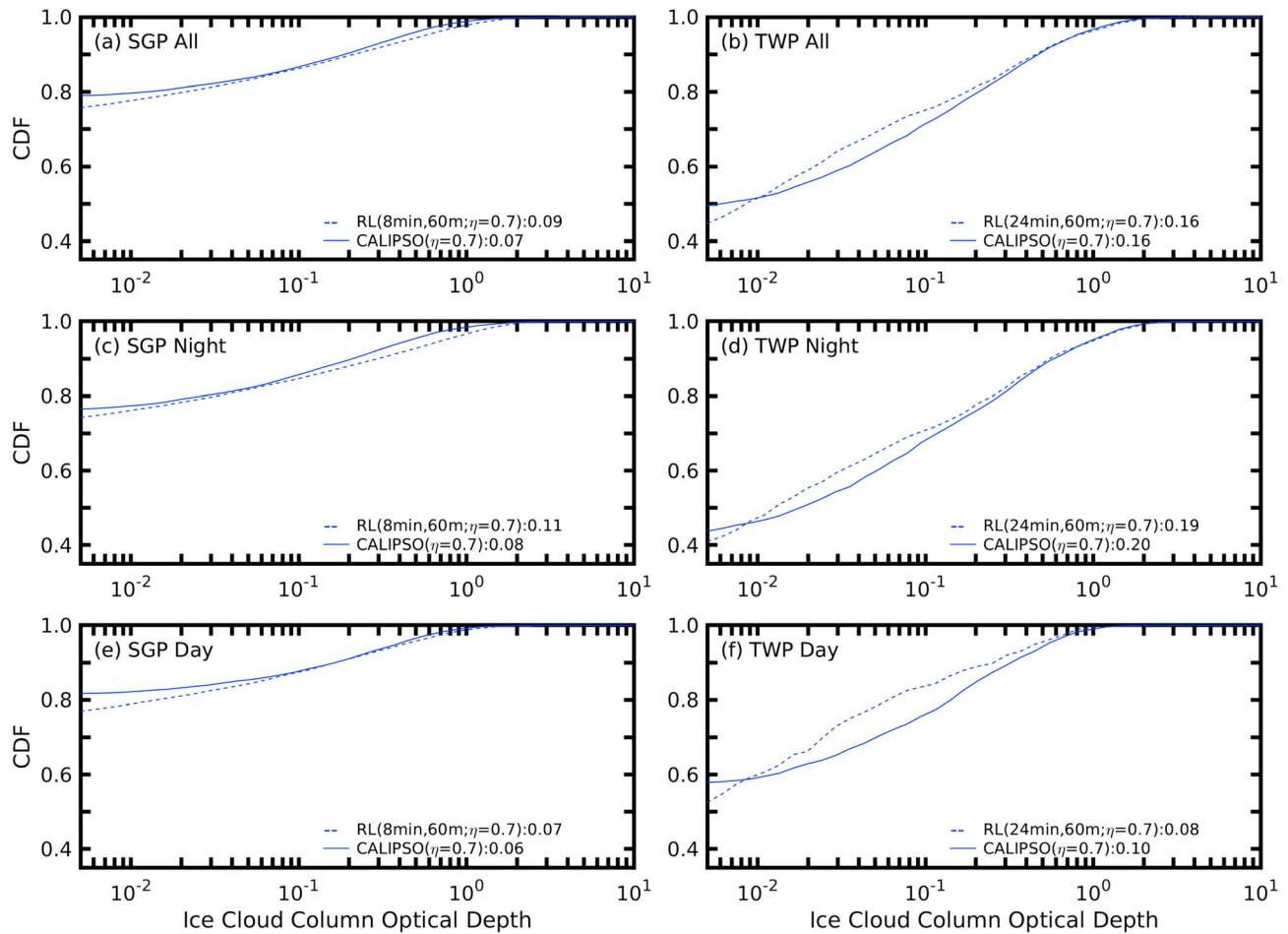


Figure 14. Cumulative distribution functions (CDFs) of ice cloud column optical depth for all the transparent collocated profiles including both ice cloudy and clear profiles when the smaller percentage of the transparent profiles from Raman lidar (RL) and Cloud-Aerosol Lidar and Infrared Pathfinder Satellite Observations (CALIPSO) is taken and the other platform's transparent profiles are thrown away in order of largest ice cloud column optical depth to match the percentage. Results are shown for CALIPSO using the CALIPSO V4 effective lidar ratio parameterization with a constant multiple scattering factor of 0.7 (blue) and the RL with extinction retrieval CALIPSO-like resolutions (i.e., 8 min/60 m at Southern Great Plains, SGP, and 24 min/60 m at Tropical Western Pacific, TWP) and lidar ratios determined by CALIPSO's Version 4 effective lidar ratio divided by a constant multiple scattering factor of 0.7 (blue dashed). SGP corresponds to the left side of the panel and TWP to the right side with all profiles on top (a and b), nighttime only profiles in the middle (c and d), and daytime only profiles on the bottom (e and f). Mean values are labeled in the legend. Data are for times collocated between the RL and CALIPSO at the SGP site from August 2008 to August 2016 and the TWP site from December 2010 to January 2015.

profiles for the platform with higher percentage of transparent profiles are then arranged in order by the ice cloud column optical depth. The transparent profiles with the largest ice cloud column optical depth are then thrown away until the percentage of transparent profiles matches the percentage of the other platform for the given collocated flyover section. For a given flyover, for example, if the RL detected 75% of profiles to be transparent and CALIPSO detected 70%, RL transparent profiles with the largest ice cloud column optical depth are thrown away until the percentage of transparent profiles becomes 70% and only these remaining profiles are considered. This is done for all flyover sections and the resultant ice cloud fraction and ice cloud column optical depth are examined to be compared with the results discussed in section 5.3.2.

After matching the percentages of collocated transparent profiles between CALIPSO and the RL, Figure 14 shows CDFs of ice cloud column optical depths from all-sky conditions (i.e., including both $\tau_{i,c} > 0$ and $\tau_{i,c} = 0$). The RL results are only shown for those using the extinction retrieval CALIPSO-like resolutions (i.e., 8 min/60 m at SGP and 24 min/60 m at TWP) and the CALIPSO temperature-dependent effective lidar ratio parameterization divided by a constant multiple scattering factor of 0.7. The CALIPSO

results are only shown for those using a constant multiple scattering factor of 0.7. Slightly lower values are noted in Figure 14 than those in Figure 13 for the corresponding distributions. This is because matching the percentage of transparent profiles overall reduces the optically thick cloud profiles used in deriving the CDFs by noting that the difference in percentages is related to the optically thick clouds. This interpretation is also supported by smaller resultant cloud fractions as the CALIPSO cloud fraction becomes 0.22 (0.52) and the RL cloud fraction becomes 0.30 (0.69) for SGP (TWP). The cloud fraction differences between the RL and CALIPSO are similar to those from Table 4, which is largely related to the optically very thin ice clouds observed by the RL. For TWP, using more consistent transparent profiles between the CALIPSO and RL leads to agreement in the all-sky mean ice cloud column optical depths between CALIPSO and the RL (see Figure 14 vs. Figure 13). For SGP, the relative difference in the all-sky means is -22% . These relative differences are much smaller than those from Figure 1 in addition to a much better agreement in the corresponding CDFs between CALIPSO and the RL (Figure 14 vs. Figure 12). Furthermore, a smaller mean column optical depth from CALIPSO than the RL under all-sky conditions is expected by noting that the CALIPSO has $\tau_{i,c} = 0$ for optically very thin ice clouds. Therefore, we can conclude that the differences in ice cloud column optical depth distributions and their mean values between the CALIPSO and the RL can be reconciled over both SGP and TWP after accounting for the averaging resolutions, lidar ratios along with the CALIPSO multiple scattering factor treatment, sensitivity to optically very thin ice clouds, and definition of transparent profiles.

6. Summary

Ice cloud lidar ratios and optical depths from spaceborne CALIPSO and ground-based RLs are compared at the ARM SGP site for 8 years and at the ARM TWP site for 4 years. Based on RL observations at both sites, the Raman and transmission methods produce very similar ice cloud lidar ratios when the two methods are applied to the same ice cloud layers. Using the RL directly retrieved lidar ratios along with temperatures from radiosonde, it is shown that ice cloud lidar ratios varied little with temperature at both SGP and TWP. This does not support the CALIPSO parameterization of ice cloud lidar ratio that increases with temperature although the CALIPSO parameterization is within the interquartile range of the lidar ratios at TWP from the RL transmission method. When combining the CALIPSO-constrained retrievals of effective lidar ratios and RL transmission-retrieved lidar ratios, the resultant multiple scattering factor was largely invariant with temperature with a value of ~ 0.7 for both SGP and TWP. This is different from CALIPSO's parameterization of multiple scattering factor, which decreases nonlinearly with temperature.

The effects of lidar ratios and averaging resolutions on the RL-retrieved ice cloud column optical depths were examined for transparent ice cloudy profiles. Three different lidar ratio scenarios are considered: the best estimate from the RL FEX, the CALIPSO V4 temperature-dependent lidar ratio parameterization, and the lidar ratios determined from the CALIPSO V4 effective lidar ratio parameterization divided by a constant multiple scattering factor of 0.7. Different RL resolutions were considered including the resolutions of 8 min/60 m over SGP and 24 min/60 m over TWP to perform the extinction retrievals at CALIPSO-like resolutions. It is found that the ice cloud column optical depth is more sensitive to lidar ratio at SGP but more to the averaging resolution at TWP.

A comparison of ice cloud detection between CALIPSO and the RLs was made for transparent collocated profiles. A feature detection CALIPSO-like temporal averaging resolution was used for the RL, which was derived from the mean CALIPSO horizontal averaging profile divided by radiosonde wind profiles, with the same vertical resolution of 60 m for CALIPSO and RLs. It was found that the RLs detect more ice clouds overall. The comparison of cloud occurrence vertical profiles shows general agreement between the RL and CALIPSO, particularly during the nighttime at TWP with feature detection CALIPSO-like resolution. Cloud occurrences for the RLs are higher than CALIPSO at both SGP and TWP during the daytime.

The comparison of ice cloud column optical depths shows that the mean ice cloud column optical depths from CALIPSO are 78% (63%) larger than those from the RLs at SGP (TWP) for collocated transparent ice cloudy profiles. These differences are partly related to differences in lidar ratios and averaging resolutions. For CDFs of ice cloud column optical depths under ice cloudy conditions, good agreement exists for $\tau > 0.3$ when the extinction retrieval CALIPSO-like resolution and the same lidar ratios were used. Overall, the RL observes more optically thin ice clouds than CALIPSO because of a higher sensitivity. By

comparing ice cloud column optical depths for collocated transparent profiles under all-sky conditions, the resultant ice cloud column optical depths CDFs show good agreement, especially when consistent resolution and lidar ratios are used. The impact of using more consistent transparent profiles between the RL and CALIPSO are also examined by matching the percentage of collocated transparent profiles for each flyover. It is found that when the percentage is matched to the lower transparent percentage, the resultant all-sky mean is more consistent between CALIPSO and the RL. This highlights the role of a transparent definition in the comparison of the RL and CALIPSO ice cloud optical depth.

This study shows that the differences in ice cloud column optical depth between CALIPSO and the RL can be largely explained by the differences in the lidar ratio, averaging resolutions, instrument sensitivity, and transparent definitions. The temperature-dependent parameterization of ice cloud lidar ratio and multiple scattering factor implemented in CALIPSO Version 4 data product was not supported by the RL lidar ratio observations. It is our future research goal to understand the differences in lidar ratios between CALIPSO and the RLs and the impact on ice cloud radiative effects. The impact of averaging resolution and the increased sensitivity for ice cloud detection on ice cloud radiative effects will also be assessed. The present study indicates that the ground-based RLs that have high sensitivity and provide direct measurements of lidar ratios can provide a useful evaluation of the CALIPSO retrievals. This will ultimately lead to a much improved CALIPSO global data product that is essential to understand the role of ice clouds in the global energy budget and climate system as a whole.

Appendix A: Ice Cloud Effective Radius

FEX takes into account multiple scattering effects using a multiple scattering model (Hogan, 2006). The multiple scattering model requires particle size for features detected to calculate the enhancement due to multiple scattering. In Thorsen and Fu (2015), the ice particle size was determined from a power law fit between effective radius and particulate extinction based on in situ data from Table 2 of Fu (1996). In this study, the ice particle size is instead determined from a relationship between effective diameter and temperature from

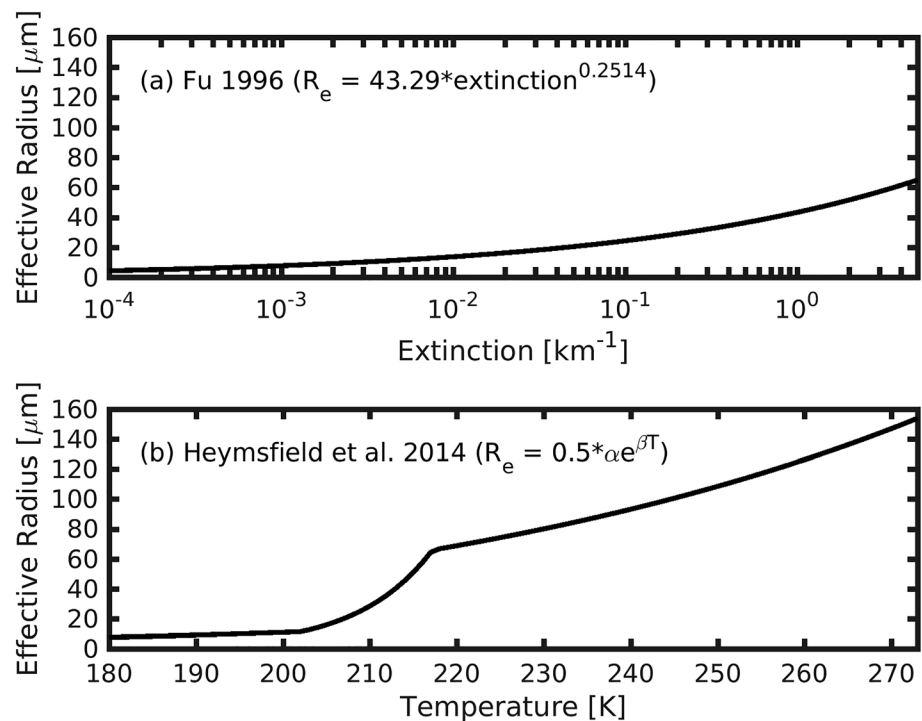


Figure A1. Ice cloud effective radius parameterizations (a) with extinction based on Fu (1996) and (b) with temperature following Heymsfield et al. (2014). The parameterization forms relating effective radius and extinction or temperature are given in the graph.

in situ data in Heymsfield et al. (2014). Here we detail the differences in ice cloud effective radius and the overall implications on the retrieved ice cloud lidar ratio, particulate backscatter and particulate extinction.

The ice cloud parameterizations of effective radius from Fu (1996) and Heymsfield et al. (2014) are plotted in Figure A1. The effective radius developed from Fu (1996) increases with increasing ice cloud particulate extinction. The effective radius developed in Heymsfield et al. (2014) increases with increasing ice cloud temperature. The effective diameter relationship with temperature outlined in Heymsfield et al. (2014) includes different coefficients for different temperature ranges (see their equation 9). Additionally, the relationship between effective diameter and temperature presented in Heymsfield et al. (2014) were specified for temperatures ranging from 188 to 273 K. To incorporate all ice cloud observations from the RL, we extended the exponential fit for the lowest temperature range to ice clouds retrieved below 188 K.

The PDFs for effective radius and retrieved lidar ratio, particulate backscatter and particulate extinction using the effective radius parameterizations based on Fu (1996) and Heymsfield et al. (2014) are plotted in Figure A2. Comparing the results using Heymsfield et al. (2014) to those from using Fu (1996), the effective radius increased greatly (Figures A2a and A2b). The larger particle sizes induce a larger multiple scattering effect. This results in larger ice cloud lidar ratios and particulate extinction and relatively similar particulate

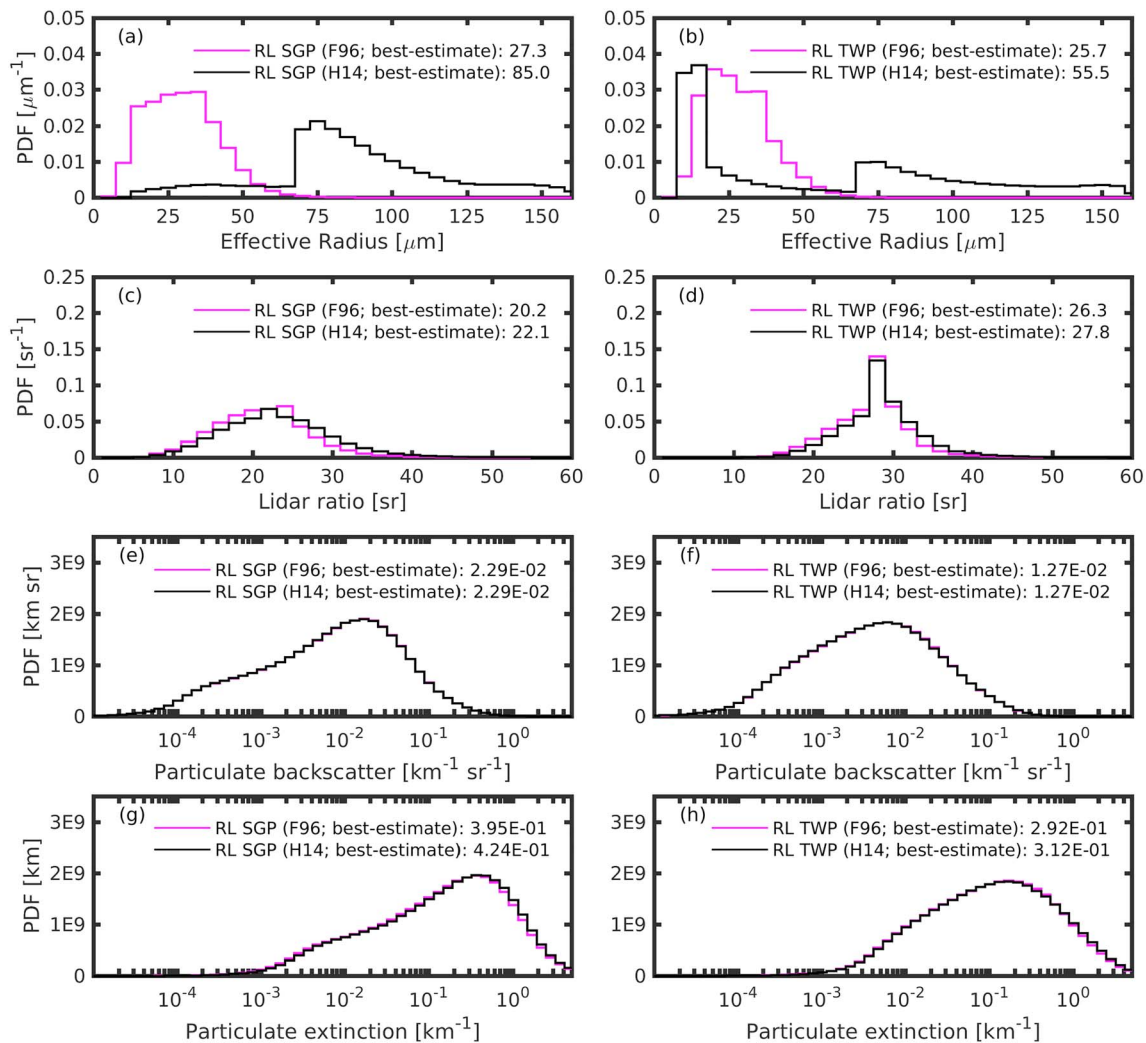


Figure A2. Probability distribution functions (PDFs) of (a, b) effective radius, (c, d) lidar ratio, (e, f) particulate backscatter, and (g, h) particulate extinction using the ice cloud effective radius parameterization based on Fu (1996; F96; magenta) and from Heymsfield et al. (2014; H14; black). Mean values are given in the legend. Data are for all best estimate ice cloud observations at the SGP site (right: a, c, e, and g) from August 2008 to August 2016 and the TWP site (left: b, d, f, and h) from December 2010 to January 2015. SGP = Southern Great Plains; TWP = Tropical Western Pacific.

backscatter. The median percent difference for the particulate extinction is 8.8% (3.4%) and for the lidar ratio is 8.7% (4.9%) at SGP (TWP). The median percent difference for the particulate backscatter is less than 0.1% at both SGP and TWP. Despite small effects, we utilize the updated relationship that is based on more recent in situ data to determine the ice particle size in this present study.

Acknowledgments

The Raman lidar RL-FEX can be downloaded from the ARM data archive (www.arm.gov/data) as an evaluation value-added product (VAP). The CALIPSO data sets were downloaded from the NASA Langley Research Center Atmospheric Science Data Center (https://eosweb.larc.nasa.gov/project/calipso/calipso_table). We thank D. M. Winker for discussions on CALIPSO's ice cloud products. We also thank M. Vaughan and J. Campbell for providing detailed reviews that greatly improved this work. This research was supported by the Office of Science (BER), U.S. Department of Energy under grant DE-SC0018190 and by NASA grant NNX16AO95G.

References

- Ackerman, T. P., & Stokes, G. M. (2003). The Atmospheric Radiation Measurement Program. *Physics Today*, *56*(1), 38–44. <https://doi.org/10.1063/1.1554135>
- Ansmann, A., Riebesell, M., & Weitkamp, C. (1990). Measurement of atmospheric aerosol extinction profiles with a Raman lidar. *Optics Letters*, *15*(13), 746–748. <https://doi.org/10.1364/OL.15.000746>
- Boudala, F. S., Isaac, G. A., Fu, Q., & Cober, S. G. (2002). Parameterization of effective ice particle size for high-latitude clouds. *International Journal of Climatology*, *22*(10), 1267–1284. <https://doi.org/10.1002/joc.774>
- Campbell, J. R., Hlavka, D. L., Welton, E. J., Flynn, C. J., Turner, D. D., Spinhrne, J. D., et al. (2002). Full-time, eye-safe cloud and aerosol lidar observation at Atmospheric Radiation Measurement program sites: Instruments and data processing. *Journal of Atmospheric and Oceanic Technology*, *19*(4), 431–442. [https://doi.org/10.1175/1520-0426\(2002\)019<0431:FTESCA>2.0.CO;2](https://doi.org/10.1175/1520-0426(2002)019<0431:FTESCA>2.0.CO;2)
- Chen, W.-N., Chiang, C.-W., & Nee, J.-B. (2002). Lidar ratio and depolarization ratio for cirrus clouds. *Applied Optics*, *41*(30), 6470–6476. <https://doi.org/10.1364/AO.41.006470>
- Davis, S., Hlavka, D., Jensen, E., Rosenlof, K., Yang, Q., Schmidt, S., et al. (2010). In situ and lidar observations of tropopause subvisible cirrus clouds during TC4. *Journal of Geophysical Research*, *115*, D00J17. <https://doi.org/10.1029/2009JD013093>
- Ferrare, R., Turner, D., Clayton, M., Schmid, B., Redemann, J., Covert, D., et al. (2006). Evaluation of daytime measurements of aerosols and water vapor made by an operational Raman lidar over the Southern Great Plains. *Journal of Geophysical Research*, *111*, D05S08. <https://doi.org/10.1029/2005JD005836>
- Fu, Q. (1996). An Accurate Parameterization of the Solar Radiative Properties of Cirrus Clouds for Climate Models. *Journal of Climate*, *9*(9), 2058–2082. [https://doi.org/10.1175/1520-0442\(1996\)009<2058:AAPOTS>2.0.CO;2](https://doi.org/10.1175/1520-0442(1996)009<2058:AAPOTS>2.0.CO;2)
- Fu, Q., Baker, M., & Hartmann, D. L. (2002). Tropical cirrus and water vapor: an effective Earth infrared iris feedback? *Atmospheric Chemistry and Physics*, *2*, 31–37.
- Fu, Q., Hu, Y., & Yang, Q. (2007). Identifying the top of the tropical tropopause layer from vertical mass flux analysis and CALIPSO lidar cloud observations. *Geophysical Research Letters*, *34*, L14813. <https://doi.org/10.1029/2007GL030099>
- Fu, Q., & Liou, K. N. (1993). Parameterization of the radiative properties of cirrus clouds. *Journal of the Atmospheric Sciences*, *50*(13), 2008–2025. [https://doi.org/10.1175/1520-0469\(1993\)050<2008:POTRPO>2.0.CO;2](https://doi.org/10.1175/1520-0469(1993)050<2008:POTRPO>2.0.CO;2)
- Garnier, A., Pelon, J., Vaughan, M. A., Winker, D. M., Trepte, C. R., & Dubuisson, P. (2015). Lidar multiple scattering factors inferred from CALIPSO lidar and IIR retrievals of semi-transparent cirrus cloud optical depths over oceans. *Atmospheric Measurement Techniques*, *8*(7), 2759–2774. <https://doi.org/10.5194/amt-8-2759-2015>
- Goldsmith, J. E. M., Blair, F. H., Bisson, S. E., & Turner, D. D. (1998). Turn-key Raman lidar for profiling atmospheric water vapor, clouds, and aerosols. *Applied Optics*, *37*(21), 4979–4990. <https://doi.org/10.1364/AO.37.004979>
- Gouveia, D. A., Barja, B., Barbosa, H. M. J., Seifert, P., Baars, H., Pauliquevis, T., & Artaxo, P. (2017). Optical and geometrical properties of cirrus clouds in Amazonia derived from 1 year of ground-based lidar measurements. *Atmospheric Chemistry and Physics*, *17*(5), 3619–3636. <https://doi.org/10.5194/acp-17-3619-2017>
- Heymsfield, A., Winker, D., Avery, M., Vaughan, M., Diskin, G., Deng, M., et al. (2014). Relationships between ice water content and volume extinction coefficient from in situ observations for temperatures from 0° to –86°C: Implications for spaceborne lidar retrievals. *Journal of Applied Meteorology and Climatology*, *53*(2), 479–505. <https://doi.org/10.1175/JAMC-D-13-087.1>
- Heymsfield, A. J., Krämer, M., Luebke, A., Brown, P., Cziczo, D. J., Franklin, C., et al. (2017). Cirrus clouds. *Meteorological Monographs*, *58*, 2.1–2.26. <https://doi.org/10.1175/AMSMONOGRAPHIS-D-16-0010.1>
- Hogan, R. J. (2006). Fast approximate calculation of multiply scattered lidar returns. *Applied Optics*, *45*(23), 5984–5992. <https://doi.org/10.1364/AO.45.005984>
- Hollars, S., Fu, Q., Comstock, J., & Ackerman, T. (2004). Comparison of cloud-top height retrievals from ground-based 35 GHz MCR and GMS-5 satellite observations at ARM TWP Manus site. *Atmospheric Research*, *72*(1–4), 169–186. <https://doi.org/10.1016/j.atmosres.2004.03.015>
- Holz, R. E., Platnick, S., Meyer, K., Vaughan, M., Heidinger, A., Yang, P., et al. (2016). Resolving ice cloud optical thickness biases between CALIOP and MODIS using infrared retrievals. *Atmospheric Chemistry and Physics*, *16*(8), 5075–5090. <https://doi.org/10.5194/acp-16-5075-2016>
- Liou, K.-N. (1986). Influence of cirrus clouds on weather and climate processes: A global perspective. *Monthly Weather Review*, *114*(6), 1167–1199. [https://doi.org/10.1175/1520-0493\(1986\)114<1167:IOCCOW>2.0.CO;2](https://doi.org/10.1175/1520-0493(1986)114<1167:IOCCOW>2.0.CO;2)
- Newsom, R. K. (2009). Raman lidar (RL) handbook. Tech. Rep. DOE/SC-ARM/TR-038. U.S. Dep. Of Energy, Washington, DC.
- Platt, C. M. R. (1973). Lidar and radiometric observations of cirrus clouds. *Journal of the Atmospheric Sciences*, *30*(6), 1191–1204. [https://doi.org/10.1175/1520-0469\(1973\)030<1191:LAROOC>2.0.CO;2](https://doi.org/10.1175/1520-0469(1973)030<1191:LAROOC>2.0.CO;2)
- Platt, C. M. R., & Dille, A. C. (1981). Remote sounding of high clouds. IV: Observed temperature variations in cirrus optical properties. *Journal of the Atmospheric Sciences*, *38*(5), 1069–1082. [https://doi.org/10.1175/1520-0469\(1981\)038<1069:RSOHC>2.0.CO;2](https://doi.org/10.1175/1520-0469(1981)038<1069:RSOHC>2.0.CO;2)
- Platt, C. M. R., & Harshvardhan (1988). Temperature dependence of cirrus extinction: Implications for climate feedback. *Journal of Geophysical Research*, *93*(D9), 11051. <https://doi.org/10.1029/JD093iD09p11051>
- Sassen, K., & Campbell, J. R. (2001). A Midlatitude cirrus cloud climatology from the Facility for Atmospheric Remote Sensing. Part I: Macrophysical and synoptic properties. *Journal of the Atmospheric Sciences*, *58*(5), 481–496. [https://doi.org/10.1175/1520-0469\(2001\)058<0481:AMCCCF>2.0.CO;2](https://doi.org/10.1175/1520-0469(2001)058<0481:AMCCCF>2.0.CO;2)
- Sassen, K., Wang, Z., & Liu, D. (2008). Global distribution of cirrus clouds from CloudSat/Cloud-Aerosol Lidar and Infrared Pathfinder Satellite Observations (CALIPSO) measurements. *Journal of Geophysical Research*, *113*, D00A12. <https://doi.org/10.1029/2008JD009972>
- Seifert, P., Ansmann, A., Müller, D., Wandinger, U., Althausen, D., Heymsfield, A. J., et al. (2007). Cirrus optical properties observed with lidar, radiosonde, and satellite over the tropical Indian Ocean during the aerosol-polluted northeast and clean maritime southwest monsoon. *Journal of Geophysical Research*, *112*, D17205. <https://doi.org/10.1029/2006JD008352>

- Stephens, G. L., Tsay, S.-C., Stackhouse, P. W., & Flatau, P. J. (1990). The relevance of the microphysical and radiative properties of cirrus clouds to climate and climatic feedback. *Journal of the Atmospheric Sciences*, *47*(14), 1742–1754. [https://doi.org/10.1175/1520-0469\(1990\)047<1742:TROTMA>2.0.CO;2](https://doi.org/10.1175/1520-0469(1990)047<1742:TROTMA>2.0.CO;2)
- Thorsen, T. J., & Fu, Q. (2015). Automated retrieval of cloud and aerosol properties from the ARM Raman lidar. Part II: Extinction. *Journal of Atmospheric and Oceanic Technology*, *32*(11), 1999–2023. <https://doi.org/10.1175/JTECH-D-14-00178.1>
- Thorsen, T. J., Fu, Q., & Comstock, J. (2011). Comparison of the CALIPSO satellite and ground-based observations of cirrus clouds at the ARM TWP sites. *Journal of Geophysical Research*, *116*, D21203. <https://doi.org/10.1029/2011JD015970>
- Thorsen, T. J., Fu, Q., Comstock, J. M., Sivaraman, C., Vaughan, M. A., Winker, D. M., & Turner, D. D. (2013). Macrophysical properties of tropical cirrus clouds from the CALIPSO satellite and from ground-based micropulse and Raman lidars. *Journal of Geophysical Research: Atmospheres*, *118*, 9209–9220. <https://doi.org/10.1002/jgrd.50691>
- Thorsen, T. J., Fu, Q., Newsom, R. K., Turner, D. D., & Comstock, J. M. (2015). Automated retrieval of cloud and aerosol properties from the ARM Raman lidar. Part I: Feature detection. *Journal of Atmospheric and Oceanic Technology*, *32*(11), 1977–1998. <https://doi.org/10.1175/JTECH-D-14-00150.1>
- Vaughan, M. A., Powell, K. A., Winker, D. M., Hostetler, C. A., Kuehn, R. E., Hunt, W. H., et al. (2009). Fully automated detection of cloud and aerosol layers in the CALIPSO lidar measurements. *Journal of Atmospheric and Oceanic Technology*, *26*(10), 2034–2050. <https://doi.org/10.1175/2009JTECHA1228.1>
- Winker, D. M., Pelon, J., Coakley, J. A., Ackerman, S. A., Charlson, R. J., Colarco, P. R., et al. (2010). The CALIPSO mission: A global 3D view of aerosols and clouds. *Bulletin of the American Meteorological Society*, *91*(9), 1211–1230. <https://doi.org/10.1175/2010BAMS3009.1>
- Winker, D. M., Vaughan, M. A., Omar, A., Hu, Y., Powell, K. A., Liu, Z., et al. (2009). Overview of the CALIPSO mission and CALIOP data processing algorithms. *Journal of Atmospheric and Oceanic Technology*, *26*(11), 2310–2323. <https://doi.org/10.1175/2009JTECHA1281.1>
- Yang, Q., Fu, Q., & Hu, Y. (2010). Radiative impacts of clouds in the tropical tropopause layer. *Journal of Geophysical Research*, *115*, D00H12. <https://doi.org/10.1029/2009JD012393>
- Yorks, J. E., Hlavka, D. L., Hart, W. D., & McGill, M. J. (2011). Statistics of cloud optical properties from airborne lidar measurements. *Journal of Atmospheric and Oceanic Technology*, *28*(7), 869–883. <https://doi.org/10.1175/2011JTECHA1507.1>
- Young, S. A., & Vaughan, M. A. (2009). The retrieval of profiles of particulate extinction from cloud-aerosol lidar infrared pathfinder satellite observations (CALIPSO) data: Algorithm description. *Journal of Atmospheric and Oceanic Technology*, *26*(6), 1105–1119. <https://doi.org/10.1175/2008JTECHA1221.1>
- Young, S. A., Vaughan, M. A., Garnier, A., Tackett, J. L., Lambeth, J. B., & Powell, K. A. (2018). Extinction and optical depth retrievals for CALIPSO's version 4 data release. *Atmospheric Measurement Techniques Discussions*, *1*(10), 5701–5727. <https://doi.org/10.5194/amt-11-5701-2018>